

Design and construction of a liquid state NMR spectrometer



Syed Waqar Ahmed
16120004

Syed Babar Ali School of Science and Engineering
Lahore University of Management Sciences

A thesis submitted for the degree of
Masters in Physics

2018

This thesis is dedicated to
my family who stood strong in support
and to the most special person,
My MUM.

Acknowledgements

First and foremost, all praise is to my Almighty God *who taught me... what I never knew*. Secondly, clinging on to His blessings I pray best for everyone who has been of any kind of assistance in my journey towards this goal. I appreciate the patience of my family with deepest urge to serve them in the coming future and I dedicate this work to them. The completion of this thesis could not have been possible without the assistance of my supervisor, Dr. M. Sabieh Anwar and his patience towards my clumsiness. I sincerely appreciate and gratefully acknowledge the perpetual assistance of Mr. M. Shafique throughout the project.

Furthermore, I pay my humble gratitude to LUMS “National Outreach Program” (NOP) in their financial assistance for this MS program. I cannot express my deep appreciation and indebtedness particularly to NOP. The thought of ever going through this exhilarating experience never crossed my mind and then, I experienced it!. I stand in debt to all my friends who supported me, motivated me and occasionally wasted my time. I also would like to use this moment to capture in memory a different kind of friend; Ma’am Sadia Babar who showed me the meaning of ”destiny”. I’d like to list a my batch mates just for the reason of having this great opportunity of knowing them; Zain (a friend), Asif (destined for good and responsible for raising class average), Junaid (the curious one), Abdullah (my imagina(ry)tive roommate), Aisha baji (a friend of God), Muwahid (a cool guy) & Zaid Saeed Khan (looking up to him).

Lastly, I wish everyone of my batch mates a success throughout their lives and well beyond that to the infinitum.

Abstract

In this work we have designed and built a modular, customizable, low-cost and high-accuracy mixed analog-digital low-field NMR spectrometer. The operating frequency ranges between 18 and 24 MHz depending on the two kinds of magnets we have employed. This apparatus can further be improved in its abilities in future for the hyperpolarized chemical physics studies which is the next stage of the project. The developed setup has advantage of low development cost and portability with reliable signal detection and reproducible results with applications for benchtop or mobile magnetic resonance.

The design utilizes permanent magnets (0.44 T or 0.55 T) for generating static field while frequency synthesis, pulse generation and reception is performed via software-based frequency synthesizers and high speed oscilloscopes. The complete analog circuit comprises various components such as an RF transmitter with variable gain, transmitter enabling circuit and circuits for superheterodyne downconversion. The receiver chain is optimized for low-noise operation allowing the capability of picking up signals from test tubes of our samples comprising 5-10 mL of liquid, ranging in the nanovolts to microvolts regime. Free-Induction Decay (FID) from various samples are observed.

Contents

1	Introduction	1
1.1	Motivation of the present work	1
1.2	Past work	2
2	A Brief Quantum Mechanical Description of NMR	4
2.1	Wavefunctional description of NMR	4
2.1.1	Rotating Hamiltonian	5
2.2	Density Matrix description of NMR	6
2.2.1	Operators for single spin	6
2.2.2	Rotations of density operators	7
2.2.3	Effects of pulse	7
2.3	Relaxation	9
2.3.1	Longitudinal relaxation	9
2.3.2	Transverse relaxation	9
3	Hardware Implementation of Compact NMR	11
3.1	RF Pulse generation	12
3.1.1	Pulse generation	12
3.1.2	Amplification	14
3.2	Sample, Probe and Magnet	15
3.2.1	Sample	15
3.2.2	Probe: Design and Tuning	16
3.2.3	Permanent Magnet	18
3.3	Receive chain	19
3.3.1	Isolation and RF-Amplification	19
3.3.2	Quadrature detection	21
3.3.3	Audio Amplification	22

4	Results	24
4.1	Transmit chain	25
4.1.1	Timing circuit	25
4.1.2	Transmitter amplifier	25
4.2	Receive chain	27
4.2.1	Probe	27
4.2.2	Pre-amplifier	27
4.2.3	Mixer	29
4.2.4	Audio amplifier	29
4.3	Sample results	30
4.3.1	Ethanol	31
4.3.2	Water	31
4.3.3	Toluene	32
4.4	Conclusion	32
A	Design and PCBs	33
A.0.1	Probe	33
A.0.2	PCB design	34
B	Components	35
B.0.1	List of abbreviations	35
B.0.2	List of tags	36
B.0.3	LabView probe tuning program	37
B.0.4	ICs	38
	Bibliography	41

List of Figures

2.1	T_1 relaxation curve, dictated by equation 2.21	10
2.2	T_2 relaxation curve, dictated by equation 2.23	10
3.1	Block diagram for complete setup for NMR Spectrometer.	12
3.2	Timing circuit, using PIC16F84A microprocessor chip for pulse timing adjustment. Running with a 4MHz crystal oscillator. Receiver and Transmitter enables are labeled A and B, respectively.	13
3.3	Circuit diagram for Transmitter amplifier. Label C represents the output collection point.	15
3.4	Samples used for various magnetic configurations.	15
3.5	Circuit diagram for the Probe.	16
3.6	Tuning curve for lab probe at 18 MHz.	17
3.7	Tuning curve for Maran Ultra probe at 23 MHz.	17
3.8	Permanent magnets.	18
3.9	Dual stage Receiver Pre-Amplifier. Both stages are separated by a variable resistor. points (i) and (ii) represents stage1 and stage2 outputs, respectively. Splitted signal in E and F travel to separate mixers. . .	20
3.10	Concept flow of quadrature detection in NMR spectrometer.	21
3.11	Circuit diagram of designed mixer. Label E represents one of the outputs from the receiver amplifier and G represents the mixer output. The Parallel attached R3 and C2 perform noise and high frequency filtering.	22
3.12	Circuit diagram of designed audio amplifier using 741 integrated operational amplifier. The gain adjusted to ≈ 27 and design allows for filtration of noise and higher frequencies.	23
4.1	A conceptual illustration of the NMR process.	24
4.2	Complete NMR system with Maran setup. Controlled distribution of power through power supply runs the amplifier circuits.	25

4.3	Plotted data of transmitter enable and receiver enable pulses. (a) show the transmission enable (TxEN) pulse along with rising edge of Trigger pulse. The delay between the two edges is $10\mu\text{s}$. (b) shows the receiver enabling pulse (RxEn, 5 ms) along with Trigger pulse.	26
4.4	Transmitter test input, 5 V. The input frequency is 23.88 MHz. The amplification only takes place with in the enabling pulse, i.e., $10\mu\text{s}$. .	26
4.5	Resulting amplified output of the transmitter, from point C in the circuit diagram 3.3. The amplified output is 100 V. Note that the amplification and gating of the signal are simultaneous process. . . .	27
4.6	Probe output, point D, as taken from the Maran (23MHz) magnetic setup.	28
4.7	Amplified output from stage 1, which is point (i) in figure 3.9.	28
4.8	Amplified output from stage 2, which is point (ii) in figure 3.9.	29
4.9	Mixer output in test pulse. The signal is filtered to output only the low frequency signal.	30
4.10	Amplified audio signal, this constitutes the final result as FID from the sample.	30
4.11	Free Induction Decay from ethanol sample. Plot (a) shows FID at offset 600KHz, plot (b) with offset 700KHz and plot (c) with offset 800KHz.	31
4.12	Free Induction Decay from water sample. Plot (a) shows FID at offset 600KHz, plot (b) with offset 700KHz and plot (c) with offset 800KHz.	31
4.13	Free Induction Decay from toluene sample. Plot (a) shows FID at offset 600KHz, plot (b) with offset 700KHz and plot (c) with offset 800KHz.	32
A.1	3D printed probe holder used in with PM-1055 magnet.	33
A.2	PCB design for all the components.	34
B.1	Block diagram of probe tuning LabView program.	37
B.2	MC1350 integrated circuit diagram revealing internal structure of the IC.	38

Chapter 1

Introduction

One of the best known techniques of investigation in the molecular regime is Nuclear Magnetic Resonance (NMR) spectroscopy. Being awarded the Noble Prize in 1991 this technique has come a long way in development of its spectroscopic techniques and has generated a plethora of research material in fields of chemistry, biology, pharmaceuticals and physics, just to name a few. Due to the sensitive dependence and chemical specificity to local environments of nuclei inside the sample molecules, it can be used reliably for determining the structures of macro molecules and other biologically important molecules, notably protein structures and the folding processes that lie at the very heart of life itself. Aside some of the limitations of the technique, like being unable to interact with zero moment nuclei [1], it has come a long way in developing many complex NMR experiments in dynamic, two and three dimensional NMR spectroscopy [2]. These experiments make use of different inter and intra-molecular interactions, spin decoherances and chemical shifts to study various samples. Currently, the NMR spectrometers can examine sample types in all three phases. One of the major spin-offs of this technique is Magnetic Resonance Imaging (MRI). Imaging, by NMR, makes use of the gradient style observation of the sample (many a times, in medicine, it's humans that are the samples) making it possible to investigate deep body morphologies [1, 4, 5, 6].

1.1 Motivation of the present work

In the research areas the information regarding chemical species under investigation is collected through structural characterization, chemical-shift and J-coupled resolved spectroscopy. This makes use of large magnetic field to split the eigenstates enough for a type of nuclie to make a noticeable mark in the spectra as affected by the environment. A conventional NMR spectrometer consists of a large electromagnets for

static fields. Such an equipment becomes bulky, high cost, limiting access to the researcher and the general public. It is well established that NMR spectroscopy and imaging can also be done in low, ultra low and also zero field regimes [3, 7]. But the advantages of low field NMR, beyond cheap access and equipment size, are a fundamental understanding of the underlying spin dynamics that are usually overtoned by high magnetic fields. It is well known that at low magnetic field strengths, ultra-low and zero-fields, new physical principles are opened up, revealing strong coupling and dipolar interactions without being masked by the Zeeman interaction. For example, it is possible to observe homo and heteronuclear J couplings, to reveal molecular structure, at low fields even when chemical shift information is suppressed. At low fields, relaxation rates also change drastically with the realizable possibility of slowly relaxing quantum states and long-lived hyperpolarization [8, 9, 10].

Low field techniques find application in spectroscopy, relaxometry and imaging. Relaxometry studies in the ultra-low field regime ($1\mu\text{T}$ to 1 mT) have been successfully employed [11] in brain imaging, combined with magneto-encephalographic investigations. The applications of low field NMR and MRI abound, both using Faraday detection as well as cryogenically cooled SQUID's. To cite a few examples low field NMR/MRI has been used for detection of liquid explosives [12], relaxation of liquids in porous media [13], measuring flow, diffusion and adsorption in chemical engineering processes [14], and the MRI of small animals [15]. There are also a large number of measurements performed in earth's ambient field [16, 17], including two-dimensional spectroscopy [18], three-dimensional imaging [19], measuring brine content in sea ice [20], high-resolution chemical analysis [21] and the imaging of groundwater in soil [22], to cite a few examples.

1.2 Past work

Based on the scientific importance of NMR, it should not be a surprise to encounter many sources of past work on the relevant subject. For example, Magnetic Resonance Systems Lab at Texas A & M came up with "A Desktop Magnetic Resonance Imaging System" describing a small desktop magnetic resonance system that used small permanent magnets and inexpensive RF integrated circuits [23]. The C-shaped design of the magnetic setup provided a static field of 0.21 T and an imaging region of 2 cm . Remarkable images were formed using the system. Another example includes assembly of several small Neodymium Iron Boron (NdFeB) magnet pieces and poles

to form magnetic circuits [24]. The use of such an assembly allowed for more effective homogeneity in the fields. The project [23] was done in close conjunction with the work described in A Low Cost MRI Permanent Magnet Prototype [24]. Another relevant past work for my thesis project was a NMR system developed at MIT [25]. This NMR system, allows students to do pulsed NMR experiments currently at MIT. Another fine work [26] was also produced by at MIT in the use of Field Programmable Gate Array (FPGA) to generate pulses and process the NMR signal. This work included the process of improvement over the magnetic setup to attain homogeneous field medium of 1.33 T.

Some recent advances have also come up using process-based advancements in coming over the problem of resolution with the low-field NMRs. The work in [27] describes the employment of Generalized Indirect Covariance (GIC) method to enhance the results from 2D homonuclear NMR spectra on 60 MHz Oxford tabletop NMR spectrometer. This required first to obtain pure shift one dimensional NMR spectrum then using it to build a 2D diagonal spectrum. The other 2D spectra are processed over this spectrum to obtain their pure shift version.

In this thesis work two different magnetic setups were used for the static field B_o . First is the magnetic setup provided by a conventional though obsolete spectrometer, Maran Ultra from Oxford Instrument. It produces a magnetic field of 0.55 T. Second is a permanent magnet from Metrolab Instruments, which provided a field of 0.44 T. Furthermore, all the circuits are lab-made, designed in Proteus, and milled on a PCB machine while a probe holder is 3D printed in our lab. Schematics and design files can be found in extra resources in appendix B. In the text we will first go through a brief quantum mechanical description of NMR and then describing all the hardware built, tested and techniques utilized. At the end we present some results of various samples we have taking from the final setup.

Chapter 2

A Brief Quantum Mechanical Description of NMR

2.1 Wavefunctional description of NMR

The NMR setup provides a constant magnetic field B_o using either permanent magnets or electromagnets depending on the field strength requirements for sample analysis. This magnetic field provides constant source for reference to the nuclear spin angular momenta. The electrons within the sample are also affected by this magnetic field but the excitation fields provided in NMR spectroscopy are specific only to the nuclear excitations, this limits our concern to the nuclear wavefunctions and there mixed states.

The Hamiltonian associated with the constant magnetic field is,

$$\hat{H}_z = -\gamma B_o \hat{I}_z, \quad (2.1)$$

where γ is the gyromagnetic ratio of nuclei, B_o represents the constant magnetic field and \hat{I}_z is the angular momentum operator. The subscript z represents the physical direction of magnetic field. The effects can be observed by solving the time-dependent Schrödinger equation for this form of Hamiltonian. This results into the wavefunction at time t_2 ,

$$\Psi(t_2) = e^{-i\omega t \hat{I}_z} \Psi(t_1). \quad (2.2)$$

Here, $\hat{R}_z(\phi) = e^{-i\omega t \hat{I}_z}$ is the rotation operator, rotating the state around z -axis by angle $\phi = \omega t$ and $\omega = -\gamma B_o$. The effects of this Hamiltonian on an eigenstates of \hat{H}_z , denoted by $|\alpha\rangle$ is,

$$\psi(t_2) = \hat{R}_z(\phi) |\alpha\rangle = e^{-i\omega t / 2 \hat{I}_z} |\alpha\rangle, \quad (2.3)$$

the state remains unchanged. For the superposition state,

$$|\psi(0)\rangle = \cos\left(\frac{\theta}{2}\right)|\alpha\rangle + \sin\left(\frac{\theta}{2}\right)|\beta\rangle, \quad (2.4)$$

and

$$\begin{aligned} \psi(t) &= \hat{R}_z(\phi)|\psi(0)\rangle \\ &= \cos\left(\frac{\theta}{2}\right)|\alpha\rangle + \sin\left(\frac{\theta}{2}\right)e^{i\omega_o t}|\beta\rangle. \end{aligned} \quad (2.5)$$

where, $|\alpha\rangle$ and $|\beta\rangle$ represent the two eigenstates and $e^{i\omega_o t}$ a the relative phase factor. Continuous application of this Hamiltonian constitutes the precessional motion of nuclear spin angular momenta around the magnetic field axis. The rotation operator shows that the precessional (Larmor) frequency is $\omega_o = -\gamma B_o$.

2.1.1 Rotating Hamiltonian

The source for excitation of nuclear spins in NMR is an oscillating RF magnetic field. The frequency of this perturbative fields is required to be the same as the Larmor frequency to ensure resonant excitation. Adding this oscillating factor to the static Hamiltonian generates a new rotating time-dependent hamiltonian. This extra Hamiltonian term affects spin orientations that are already set by the constant magnetic field B_o . However, the nuclear spin already rotating with the Larmor frequency only observe the perturbative field when considered in the rotating frame of reference.

By using Rotating Wave Approximation (RWA) we can safely neglect the counter rotating effects of the field (see appendix A for a discussion of RWA) The apparent frequency of the Larmor precession in this frame will be an *offset*,

$$\Omega = \omega_o - \omega_{rot.frame}. \quad (2.6)$$

In the rotating frame the reduced static field will be, $\Delta B = -\Omega/\gamma$. We can write time-independent Schrödinger equation in rotating frame by considering the remaining magnetic field component. In the lab frame, the applied oscillating RF field is given by

$$B_{RF}(t) = \frac{B_{RF}}{2}\cos(\omega_{RF}t + \phi_p)\hat{x} + \frac{B_{RF}}{2}\sin(\omega_{RF}t + \phi_p)\hat{y} \quad (2.7)$$

Thus, the perturbative Hamiltonian in the RWA will be given by,

$$\hat{H}_{RF}(t) = \frac{\omega_1}{2}\cos(\Omega t + \phi)\hat{I}_x + \sin(\Omega t + \phi)\hat{I}_y, \quad (2.8)$$

where $\omega_1 = -\gamma B_{RF}$ is called the nutation frequency.

We can write rotating frame Schrödinger equation as:

$$\frac{d}{dt} |\Psi\rangle = -i\hat{H} |\Psi\rangle \quad (2.9)$$

where, \hat{H} is the rotating frame spin hamiltonian defined as,

$$\hat{H} = \hat{R}_z(-\phi)\hat{H}\hat{R}_z(\phi) - \omega_{RF}\hat{I}_z. \quad (2.10)$$

These equations give the ingredients of deriving the dynamics of spins as viewed from the rotating frame. First term in this Hamiltonian represents the part of Hamiltonian apparently rotating around z -axis. It vanishes when perfectly in resonance, i.e. $\omega_{RF} = \omega_o$. The second term represents an additional correction to the spin dynamics, over the transformation of the spin operator.

The final total rotating hamiltonian becomes,

$$\begin{aligned} \hat{H} &= \omega_o\hat{I}_z - \omega_{ref}\hat{I}_z + \frac{\gamma B_{RF}}{2}(\cos(\phi_p)\hat{I}_x + \sin(\phi_p)\hat{I}_y) \\ &= \Omega\hat{I}_z + \frac{\gamma B_{RF}}{2}(\cos(\phi_p)\hat{I}_x + \sin(\phi_p)\hat{I}_y), \end{aligned} \quad (2.11)$$

for offset, $\Omega = 0$, the total rotating hamiltonian generates oscillation on xy plane. Equation (2.11) shows the RF pulse is frequency selective; spins with precession close to RF irradiation are significantly affected by the pulse.

2.2 Density Matrix description of NMR

To describe neatly a system we can make use of density operator approach for the spin states. Density operator approach is sufficient for single, uncoupled, spin ensemble. For coupled spins, using product of operators is more convenient. Density operator is a mathematical tool that can capture and illustrate all the details of an ensemble much efficiently.-

2.2.1 Operators for single spin

In case of non-interacting ensemble, uncoupled spins, density operators can be expressed as a linear combination of the spin angular momentum operators \hat{I}_z , \hat{I}_y and \hat{I}_x .

$$\hat{\rho}(t) = a_o\hat{I}_o + a_x\hat{I}_x + a_y\hat{I}_y + a_z\hat{I}_z. \quad (2.12)$$

where \hat{I}_o is maximally mixed state and a_x , a_y and a_z are coefficients propotional to the *ensemble average* of the coefficients of ensemble states. The time evolution of the density operators is given as

$$\hat{\rho}(t) = e^{-i\hat{H}t}\hat{\rho}(0)e^{i\hat{H}t} \quad (2.13)$$

due to the pulsed behavior of transverse perturbative field the Hamiltonian is different during the pulses and during the free precession.

$$\hat{H}_{free} = \Omega\hat{I}_z; \quad \hat{H}_{x,pulse} = \Omega\hat{I}_z + \omega_1\hat{I}_x. \quad (2.14)$$

$\omega_1 \equiv$ the RF field strength determining the rotation rate of magnetization about the field along the x-axis.

2.2.2 Rotations of density operators

We know that the density operator can be written as a linear combination of Pauli matrices, it enables us to come up with rotation of each component independent of all the others. In order to simplify the rotation schemes one can utilize the *sandwich formulas*, a well know technique in quantum mechanics. The six possible rotations are given in Table 2.1. Using vector notation one can understand these actions simply as a rotation of magnetization vectors. This analogy is complete and entirely appropriate.

Table 2.1: The sandwich formulas for the operators \hat{I}_x, \hat{I}_y and \hat{I}_z through angle θ .

Rotation about	Operator	Identity
x	\hat{I}_y	$R(-i\theta\hat{I}_x)\hat{I}_yR(-i\theta\hat{I}_x) \equiv \cos\theta\hat{I}_y + \sin\theta\hat{I}_z$
x	\hat{I}_z	$R(-i\theta\hat{I}_x)\hat{I}_zR(-i\theta\hat{I}_x) \equiv \cos\theta\hat{I}_z - \sin\theta\hat{I}_y$
y	\hat{I}_x	$R(-i\theta\hat{I}_y)\hat{I}_xR(-i\theta\hat{I}_y) \equiv \cos\theta\hat{I}_x - \sin\theta\hat{I}_z$
y	\hat{I}_z	$R(-i\theta\hat{I}_y)\hat{I}_zR(-i\theta\hat{I}_y) \equiv \cos\theta\hat{I}_z + \sin\theta\hat{I}_x$
z	\hat{I}_x	$R(-i\theta\hat{I}_z)\hat{I}_xR(-i\theta\hat{I}_z) \equiv \cos\theta\hat{I}_x + \sin\theta\hat{I}_y$
z	\hat{I}_y	$R(-i\theta\hat{I}_z)\hat{I}_yR(-i\theta\hat{I}_z) \equiv \cos\theta\hat{I}_y - \sin\theta\hat{I}_x$

2.2.3 Effects of pulse

If we consider a density matrix in the presence of static magnetic field in z -direction then the evolved density matrix state under pulsed perturbative field \hat{H}_{pulse} will gain transverse components. Let the initial state be,

$$\hat{\rho}(0) = \hat{I}_z \quad (2.15)$$

then in the rotating frame, the density matrix form after a pulse of duration t_p will be,

$$\hat{\rho}(t_p) = \cos(\omega_1 t_p) \hat{I}_z - \sin(\omega_1 t_p) \hat{I}_y. \quad (2.16)$$

This shows that the state \hat{I}_z has transformed to a state lying in the zy -plane, and is a linear combination of operators \hat{I}_z and \hat{I}_y . This can be geometrically represented as a rotation around the x -axis. After the pulse, this planar rotating density operator will evolve under the static field Hamiltonian.

$$\begin{aligned} \hat{\rho}(t_p) &\longrightarrow \hat{\rho}(t_f) \\ \hat{\rho}(t_f) &= \cos(\omega_1 t_p) \hat{I}_z - \sin(\omega_1 t_p) \cos(\Omega t) \hat{I}_y + \sin(\omega_1 t_p) \sin(\Omega t) \hat{I}_x, \end{aligned} \quad (2.17)$$

so that the $\hat{\rho}(t_f)$ is the final form of density operator with component in all three dimensions. The coefficient of the \hat{I}_y and \hat{I}_x represents the magnitudes of magnetization in each direction. This quantity can be detected and observed experimentally, which is the goal of every NMR experiment.

The signal generated, therefore, can be summarized as,

$$\begin{aligned} S_x &= S_o \sin(\omega_1 t_p) \sin(\Omega t) e^{(-t/T)} \\ S_y &= -S_o \sin(\omega_1 t_p) \cos(\Omega t) e^{(-t/T)} \end{aligned} \quad (2.18)$$

where, $e^{(-t/T)}$ is the factor included for the decay in signal with time t . The decay, firstly, is due to the ‘‘realignment’’ of the magnetization with the static Hamiltonian and secondly, due to the environmental interaction. We will see that environmental effects that are responsible for these decay in the next section. The constant T is the time constant characterizing the decay. this constant has combinations from two kinds of decay, called T_1 and T_2 .

The signal can be written in complex form for simplification. If we let the amplitude value be fixed, S_o for both components, then,

$$\begin{aligned} S(t) &= S_x + iS_y \\ &= S_o e^{i\Omega t} e^{(-t/T)}. \end{aligned} \quad (2.19)$$

Equation 2.19 represents the Free Induction Decay (FID). The generated signal picking up both S_x and S_y can also be captured by the term $Tr(\rho(t)\hat{I}^*)$, where $\hat{I}^+ = \hat{I}_x + i\hat{I}_y$.

2.3 Relaxation

At the end of a pulse the magnetization reaches the equilibrium through the process of *relaxation*. The loss in observed signal strength and the return of equilibrium state is simultaneous. Obviously, one of the agents of relaxation is inhomogeneities in the external magnetic field B_o but the lattice interaction add another parameter to the decay. Relaxation rate is also determined by molecular properties, such as shape and motion. It is found that the relaxation rates in NMR takes between milliseconds to seconds for complete relaxation of equilibrium magnetization. In extreme cases and for ^{13}C , this rate can reach upto a few minutes. The size of this equilibrium z -magnetization depends on the gyromagnetic ratio, spin density and strength of the applied field.

2.3.1 Longitudinal relaxation

The term *longitudinal relaxation* is designated to the individual relaxation process which shows restoration of equilibrium spin polarization in the presence of the static magnetic field, B_o . It is also called “ T_1 relaxation”. The spin alignment increases the M_z component of the magnetization. A simple equation can be modeled respecting the fact that the rate of relaxation to the z -component is proportional to the deviation of the bulk magnetization from its equilibrium value. The relaxation equation for this process can be written as,

$$\frac{dM_z(t)}{dt} = -R_z[M_z(t) - M_z^0] \quad (2.20)$$

$R_z(= 1/T_1)$ is rate constant for longitudinal relaxation determining the rate of approach of equilibrium. It is closely related to first order rate constant [6]. Farther the magnetization is from the equilibrium the faster will be the rate and time for the magnetization to attain equilibrium reduces as the rate constant R_z increases. Equation 2.20 can be solve to obtain,

$$M_z(t) = [M_z(0) - M_z^0]e^{-R_z t} + M_z^0. \quad (2.21)$$

2.3.2 Transverse relaxation

We can predict the relaxation of transverse magnetization, for example the x -magnetization, by a model equation:

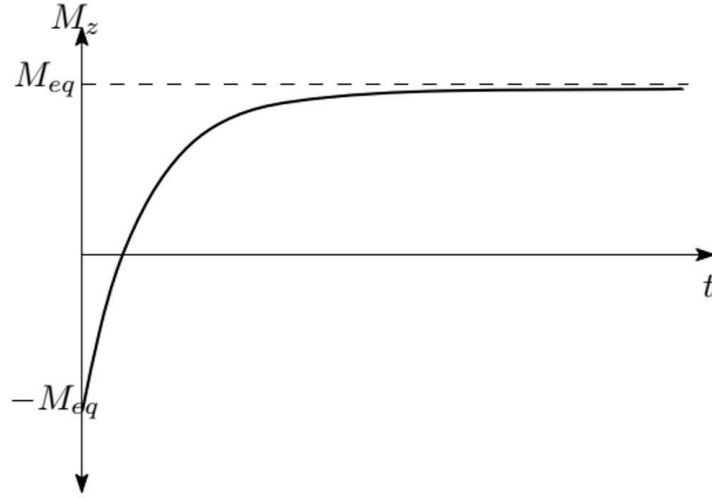


Figure 2.1: T_1 relaxation curve, dictated by equation 2.21

$$\frac{dM_z(t)}{dt} = -R_{xy}M_x(t), \quad (2.22)$$

where R_{xy} is a constant of transverse relaxation. It is a reciprocal of the time constant, $T_2 (= 1/R_{xy})$. It can be shown from equation 2.22 that the decay of x -magnetization is exponentially decreasing to zero.

$$M_x(t) = M_x(0)e^{-R_{xy}t}. \quad (2.23)$$

The decay rate is determined by R_{xy} . The same scheme is followed by y component as well.

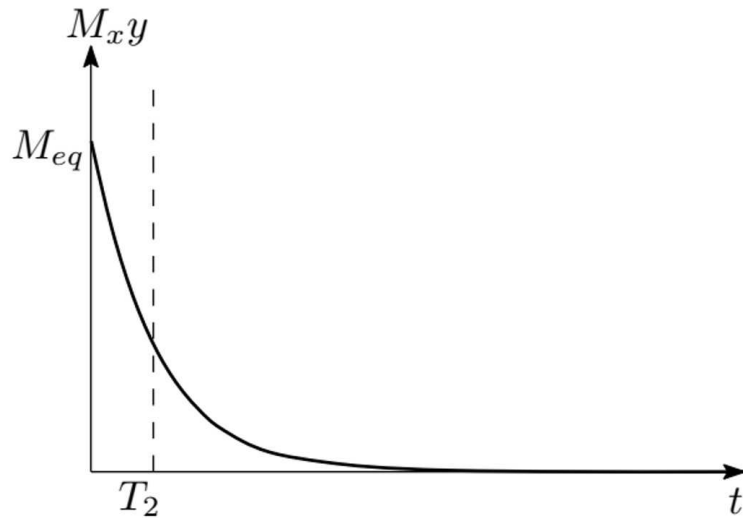


Figure 2.2: T_2 relaxation curve, dictated by equation 2.23

Chapter 3

Hardware Implementation of Compact NMR

The experimental setup for the observation of NMR response must provide methods to detect the signal from sample nuclei after being excited. This would require generation of the desired excitation signal and receiving, low-noise amplification of the signal, viewing and being able to analyze it. The entire hardware for the NMR spectrometer can be divided into four major parts,

1. Transmitter
2. Probe and Magnet
3. Receiver
4. Detection and Processing.

Figure 3.1 illustrates the basic idea of observing NMR signal. The transmitter chain will provide a gated sinusoid to introduce a perturbation. The signal could be shaped and sequenced or stand alone. Inside the sample the nuclei precess at the chemical shifted Larmor frequency $\omega_o = 2\pi f_o$ inside the constant magnetic field. The probe utilized here is actually transceiver probe which acts as transmitter during the pulse, exciting the nuclei, and works as a receiver as the pulse is off and acquisition, over the receiver side section, starts. Alternatively the behavior of the probe can be visualized as a switched antenna, transmitting RF energy in a desired pattern and receiving the RF signal section at precisely timed intervals. Because there is no induced signal at equilibrium so the only signal produced is right after a perturbation due to the nutation of nuclei and their subsequent re-alignment back to equilibrium. A noticeable signal requires amplification followed by detection and time domain

display. Some of the signals and components have been abbreviated in the following discussion. A list of abbreviations can be found in Appendix B.

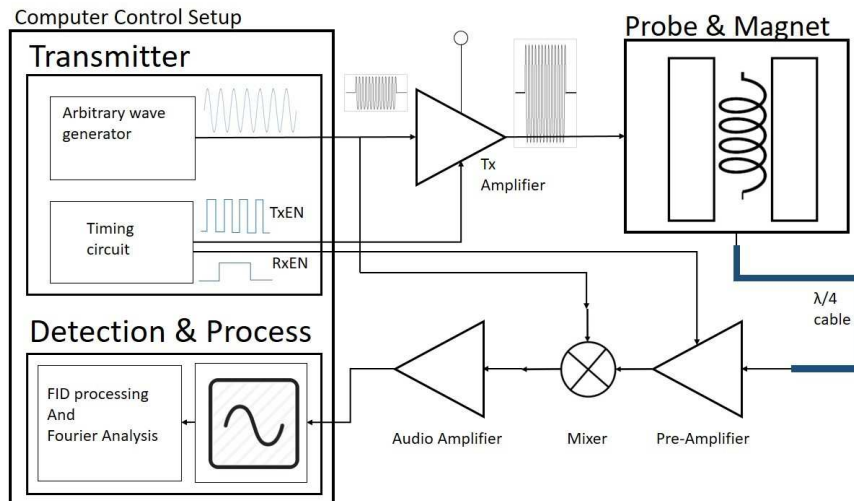


Figure 3.1: Block diagram for complete setup for NMR Spectrometer.

3.1 RF Pulse generation

The beginning of every NMR experiment requires pulse sequence which dictates the rotations of the spins. In our preliminary setup, we utilized single pulse of $10\mu\text{s}$ to achieve first hand results of Free Induction Decay (FID) but different sequence patterns can also be explored. We now describe the various components of the compact NMR spectrometer.

3.1.1 Pulse generation

The fundamental frequency, let's call it f_o , is provided by the single channel of an arbitrary waveform generator (AWG, ZT5211). This module, from ZTEC, is capable of generating arbitrary waveforms at a maximum frequency of 50 MHz and a sampling rate of 20 ns. This card is engaged with the computer through a PXI chassis (National Instruments PXIe-1073). The AWG card is controlled via ZWave software interface.

The signal is windowed by a timing circuit which runs in synchronization with the AWG by the edge of an External Trigger pulse (Trg) of arbitrary length (we used 1 ms). To achieve a full control over design of the pulse (or pulse sequence). We programmed the pulse sequence into a PIC16F84A, a programmable micro processor providing control over the pulse sequence. The AWG is set to produce a burst of

length 2 ms of frequency f_o . The minimum achievable pulse length is 40 ns and the resolution is 5 ns. The window, from timing circuit, provides sequenced blanking forming pulse sequence of desired lengths and pattern as adjusted via the programmed PIC controller. Figure 3.2 shows a circuit for generating the TxEN ($10\mu\text{s}$ pulse used in our preliminary experiments), note that even though the burst of frequency f_o coming from the AWG is 2 ms long, only $10\mu\text{s}$ of this signal is gated into the Tx amplifier. The rise and fall time for the pulse is 300ns . The timing circuit also provides enabling for receiver amplifier (RxEN) which in our experiments is a 5 ms pulse appearing after a delay of $10\mu\text{s}$ after end of final transmission pulse. A relatively large window for receiver allows to collect the signal till (almost) complete decay.

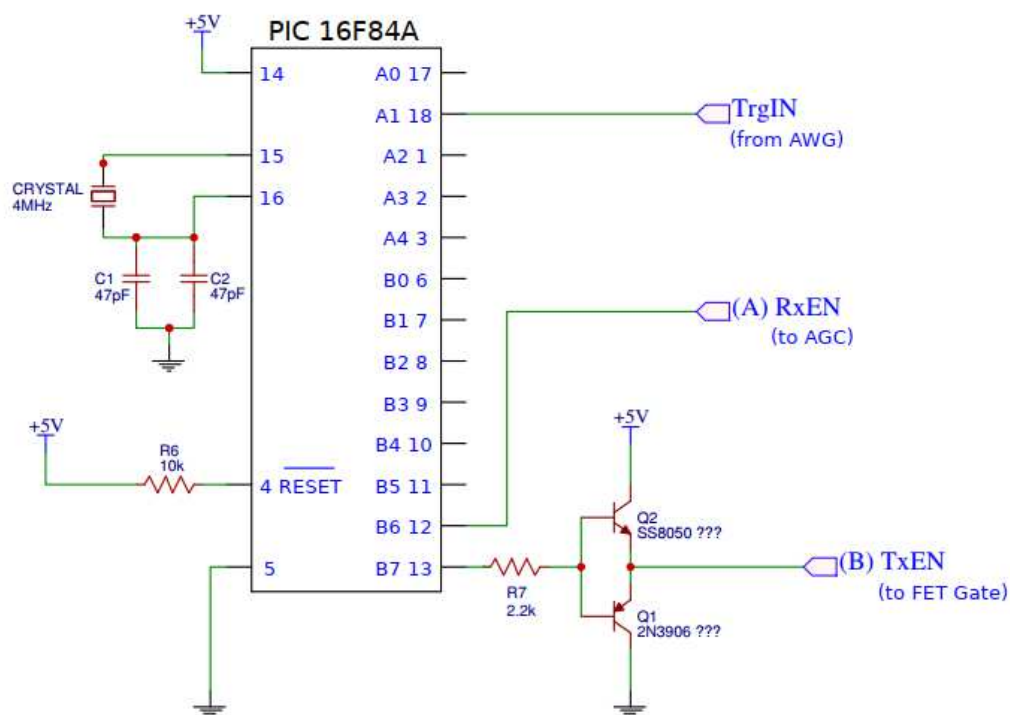


Figure 3.2: Timing circuit, using PIC16F84A microprocessor chip for pulse timing adjustment. Running with a 4MHz crystal oscillator. Receiver and Transmitter enables are labeled A and B, respectively.

Additionally, the phase of the Tx pulse, which can allow for the rotation of the spins about different axis on the Bloch sphere, is another variable parameter controlled via the AWG card. For the magnetic field strength of 0.44 T the frequency f_o is 18.73 MHz (Larmor frequency for protons) and is produced from the AWG and the offset is provided over or under this value directly from ZWave software user interface. This signal will provide the perturbative magnetic field B_1 . The various labels A, B, C, . .

. which represent the interconnections between the various electronic boards are also summarized in Appendix B.

3.1.2 Amplification

The pulse produced needs to be amplified in order to maximize the excitation inside the sample through maximizing the power delivered to the sample. Amplitude of the signal from AWG is directly controlled via ZWave software user interface. The TxEN provided to the Transmitter amplifier (TxAmp) from timing circuit programmed for desired timing and sequencing. The notable specifications of our designed TxAmp are given in Table 3.1. The design also includes noise filtration. The Schematic for the transmitter amplifier is shown in Fig 3.3. The amplifier feeds on a 24 V power supply and uses FET's embedded inside BLF184XR chip, the amplified output is collected through transformer. The major IC's used in the project are highlighted in Appendix B.

Table 3.1: Transmitter amplifier description.

Part	Description
Major IC	BLF184XR
Operating Voltage	24 V
Gain	20
Band width	10 - 100 MHz
Rise time	300 ns
Fall time	300 ns
Output power	$\approx 100W$

We can now channel this amplified signal to sample. The pulsed output is then delivered onto probe through a diode switch network which restricts the minute NMR signal to follow onto the transmitter side when transmission is blanked and reception is derived. Protection must be considered with such minute signals throughout the circuit chain. This diode switch is made of set of six 1N4007 diodes as shown in Fig 3.3.

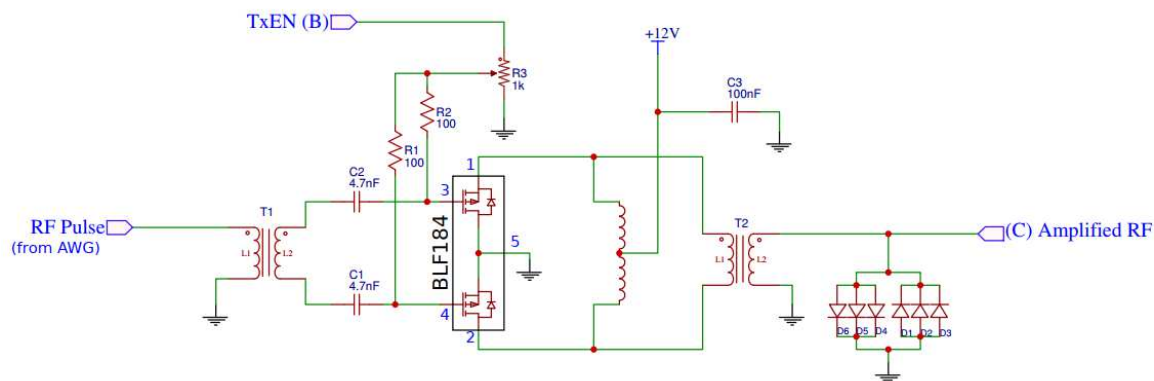


Figure 3.3: Circuit diagram for Transmitter amplifier. Label C represents the output collection point.

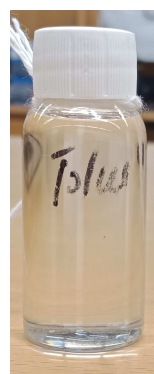
3.2 Sample, Probe and Magnet

3.2.1 Sample

The sample used is approximately 5 ml in volume sealed inside glass tube with 8 mm outer diameter, 6.5 mm inner diameter and tube length of 80 mm. This size of sample is chosen in accordance with the dimensions of the cavity available inside the permanent magnet and coil to be wrapped around the sample. The sample is at room temperature and atmospheric pressure. Because the techniques currently being used are not sensitive enough and owing to the fact that the de-excitation of nucleus causes only an extremely minute oscillating magnetic field in the coil makes it essential to use large sample size to boost the strength of the signal. Further increase in detected values of the sample is achieved by signal averaging and amplification. The test samples included water, ethanol and toluene.



(a) water, sealed inside glass tube



(b) Toluene

Figure 3.4: Samples used for various magnetic configurations.

3.2.2 Probe: Design and Tuning

In our experiments we used two different detection setups. First is a lab-made probe with permanent magnet and second is a magnet that is part of Maran Ultra NMR spectrometer (Oxford Instruments). So far, no other technique has been known to accurately deliver field pulses to the sample, then via inductor coils wrapped around the sample. The probe is essentially an RLC tank circuit with inductor playing the role of (magnetic field) provider. The RLC circuit, is a tuned to f_o and matched with the output impedance of the Tx amplifier (50Ω). This ensures maximum power transfer to and from the sample. A variable capacitor attached in the circuit design provides control for probe tuning to attain maximum response (minimum impedance). The circuit is matched to an impedance of 50Ω to minimize the power reflection.

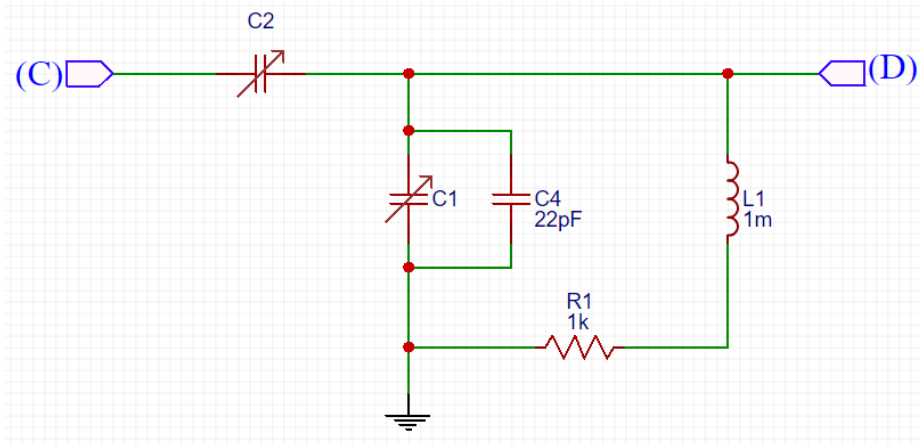


Figure 3.5: Circuit diagram for the Probe.

Table 3.2: Probe specification.

Wire gauge	1.72 mm
Coil diameter	8.80 mm
Turns	8 (hand wound)
Probe length	14.17 mm

The tuning of circuit to f_o is carried out using a LabView Program with PC interfaced oscilloscope (Agilent, DSOX2002A). The technique utilizes a directional coupler fixed with tuning circuit, arbitrary waveform generator and oscilloscope (PC interfaced). The oscilloscope picks up the reflected power from the circuit, circuit is tuned by minimizing the reflection using the combination of variable capacitors at our required frequency f_o . Probe-2 (Maran probe) is also examined for it's tuning.

Figure 3.6 AND 3.7 shows the GUI for the tuning process for each probe. This tuning to the respective Larmor frequency is vital in order to achieve high quality factor (Q) and thus high signal-to-noise ratio (SNR).

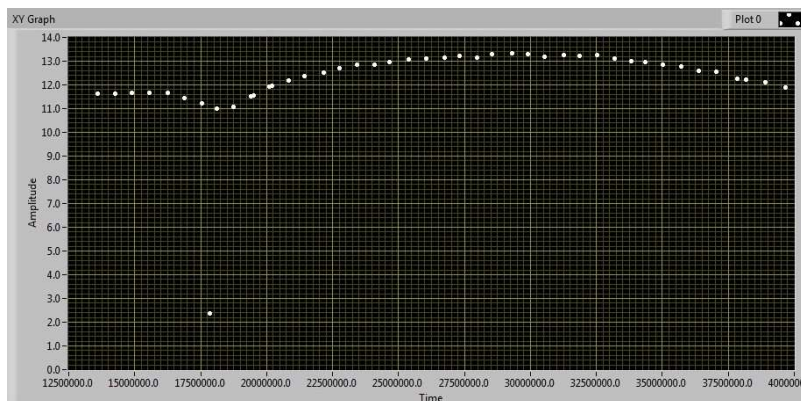


Figure 3.6: Tuning curve for lab probe at 18 MHz.

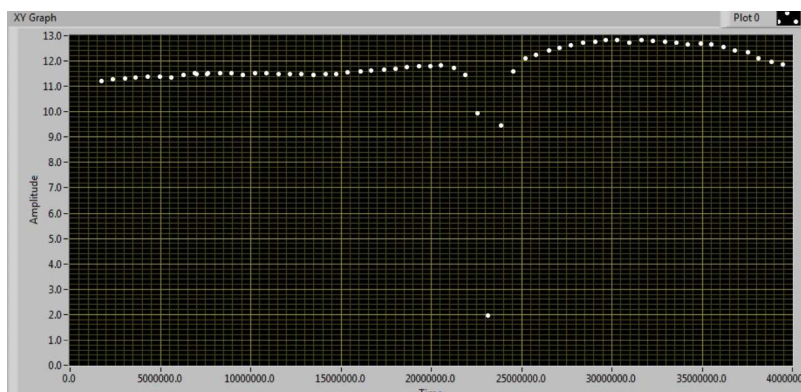


Figure 3.7: Tuning curve for Maran Ultra probe at 23 MHz.

The design for both probes is essentially the same. The inductor in the RLC circuit acting as the probe, the transceiver, holds the sample tube in the inductor cavity. The part of sample under constant magnetic field B_o which is coupled with the coil cavity is called *active region*. The properties of the inductor coil in lab-made probe are given in Table 3.2.

Under the action of alternating current the field produced inside the inductor is in linearly oscillatory fashion. Linearly polarized oscillations can be converted in linear superposition of counter rotating fields where by rotating wave approximation counter rotating direction is neglected by the precessing spin magnetizations and excitation is induced via in-phase rotating perturbative field. The de-excitation of the magnetization causes similar but damped oscillating magnetic field which induces currents in the coil and hence the signal.

3.2.3 Permanent Magnet

Typical high-field NMR experiments employ strong fixed magnetic fields B_o achieved via supercurrents in a superconducting coil that is cooled through liquid helium. Typical magnetic fields in commercial magnets range from 10 to 20 T. For lower magnetic fields however, permanent magnets are more compatible. In the current work we use two kinds of magnets. First, a permanent magnetic field of strength 0.44 T is provided through a permanent magnet (PM-1055, METROLAB Instruments) yielding a Larmor frequency of 18.73 MHz for protons. This sets the carrier frequency for the NMR design and has been incorporated into the selection of all major components in the spectrometer. The homogeneous region of the magnet cavity is 12 mm diameter. This field has been measured with the help of a Gaussmeter (410, Lakeshore).

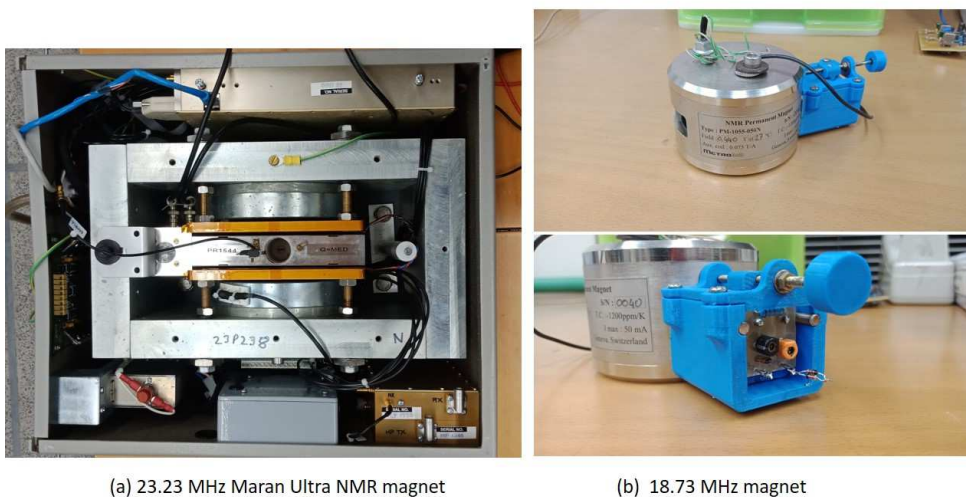


Figure 3.8: Permanent magnets.

A total open space of area of $50 \times 13 \text{ mm}(\phi \times H)$ is available at the center of magnet which houses the probe coil. For adjustments the probe module is designed and 3D printed and its position can be adjusted with the homogeneous zone of 12 mm diameter within the gap.

A second magnet, part of Maran Ultra NMR spectrometer, with magnetic field of 0.55 T. The corresponds to 23.23 MHz for protons. The magnet provides field region of $150 \times 80 \text{ mm}(\phi \times H)$ between the poles. The sample position is adjustable within the homogeneous zone of 90 mm.

3.3 Receive chain

The receive chain is based on the superheterodyne technique to filter out the signal. The filter output is minute (in the nanovolts to microvolts regime) and must be amplified by receiver amplifier. This amplification is achieved home built multiple stage amplifiers.

3.3.1 Isolation and RF-Amplification

The schematic in Fig 3.1 shows that the transmitter, probe and receiver are all connected in same line so as the RF signal approaches the probe for excitation of the nuclei it may also follow in into the receiver amplifier line which, being high power pulse, can damage the receiver amplifier. This situation is prevented by obtaining isolation between the two chains. A quarter wave cable is a coaxial cable of length specific to the signal frequency ($\lambda/4$) connected right after the probe. Quarter wave cable has the property that $Z_i Z_o = |Z|^2$ where Z_i is input impedance, Z_o is output impedance and Z is characteristic impedance of cable [5]. The quarter wave line increases the diode switch impedance resulting in apparent isolation of the first part of the cable to the second. This allows power completely to be transmitted to the probe and also secures the sensitive receiver amplifier.

The second stage of isolation is achieved when the transmitter pulse is off and the sample signal is picked up by the probe. By the same token the signal follows through both directions, on the back propagation it encounters diode switch (see Fig 3.3) which blocks the path so that the signal only has a single direction to follow, that is, to the receiver amplifier.

The integrated circuit MC1350 is used for the receiver amplifier. The amplifier is made of two stages providing a pass band of 10KHz. The gain is controllable through a variable resistor between the two stages. Figure 3.9 shows the circuit diagram of the amplifier where both stages are joined with variable resistor (R4) in the middle. The resulting signals from both stages are shown in Fig 4.6 and 4.7, respectively which we will describe later. The output from second stage is fed directly into the mixer. When the receiver gain is kept high and the amplifier allowed to run at all times it produced a problem of power-seeping and raises the signal level, resulting in the vertical skewness in the FID. One solution is to adjust the gain appropriately which would undermine the goal of maximizing the minute NMR signal. However, a second solution was utilized to make sure the gain remains controllable and also the signal level skewness diminishes as well. for this purpose we introduced a transistor switch

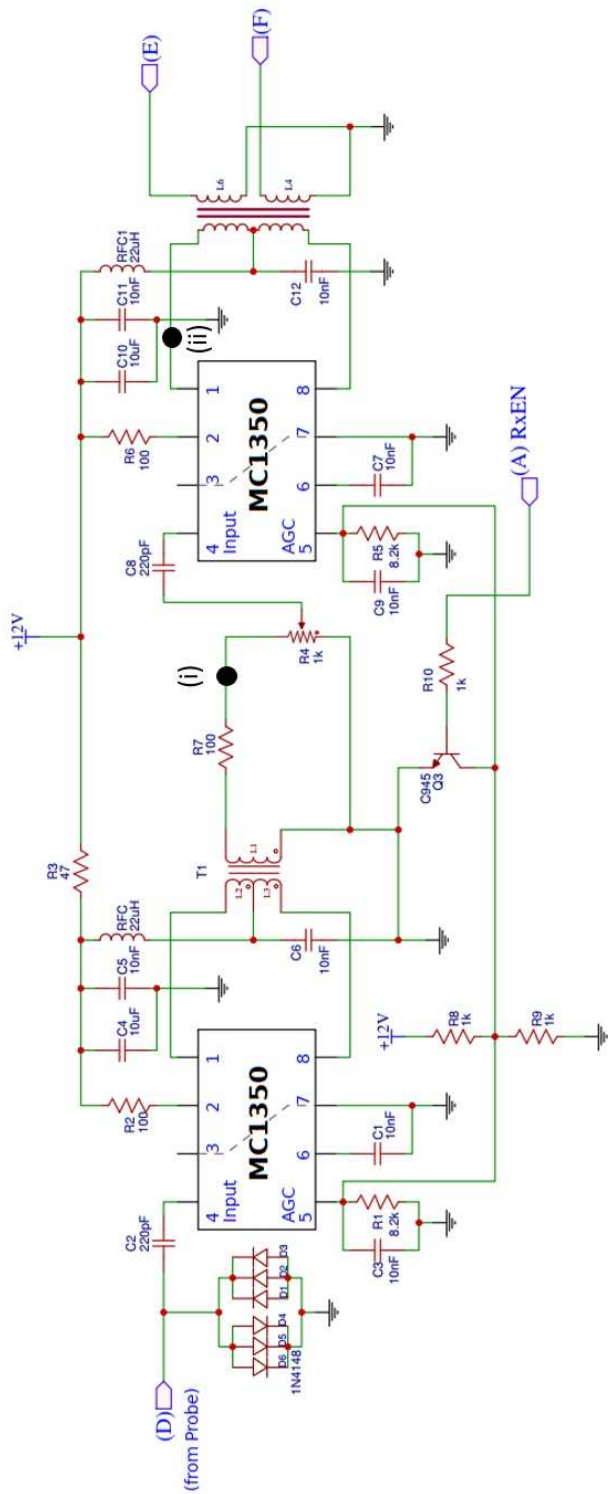


Figure 3.9: Dual stage Receiver Pre-Amplifier. Both stages are separated by a variable resistor. points (i) and (ii) represents stage1 and stage2 outputs, respectively. Splitted signal in E and F travel to separate mixers.

(Q3 shown in the Fig 3.9) synchronized with the programmable timing circuit pulse (RxEN- 2 ms) with the help of which we can turn the amplifier on only at and for the time period the user wishes to acquire the signal. This pulsed time window is called the *acquisition window*.

3.3.2 Quadrature detection

We employed quadrature detection technique used in NMR spectroscopy in our setup using second channel of (the dual-channel) AWG. This allows sign detection of the signal with respect to f_o , i.e., NMR frequencies above all and below f_o can be detected. Furthermore, this stage down converts the RF frequencies to audio, which can then be conveniently amplified and fed into an analog-to-digital converter. Figure 3.10 shows the concept flow of quadrature detection which then outputs two 90° phase shifted results that will be treated as “real” and “imaginary” inputs for Fourier analysis.

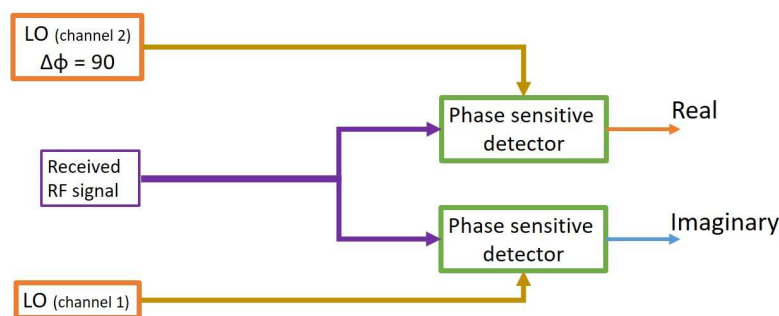


Figure 3.10: Concept flow of quadrature detection in NMR spectrometer.

To filter out the signal from total received signal we employed two mixers with two separate channels from AWG. The two frequencies that the mixer takes in are receiver reference frequency at LO port of the mixer and signal (in MHz) at RF port E of the mixer. Both signal outputs are at the same frequency but shifted phases. Mixer circuit simply multiplies the two input frequencies, i.e, the Local Oscillator (LO) from AWG with the received RF signal at E (in Fig ??), and outputs the results in the sum and difference of the two frequencies. By filtering out the lower frequency for total signal the digital conversion becomes fairly simple. This is equivalent to observing the signal in rotating frame [6]. Typical downconverted NMR signal frequencies range in KHz, the difference output of the mixer therefore becomes useful and is filtered

and further amplified by audio amplifier. Fig 3.11 shows the schematic of a single mixer. At the end, the summed output (higher frequency) is drained to the ground and differenced output propagates along.

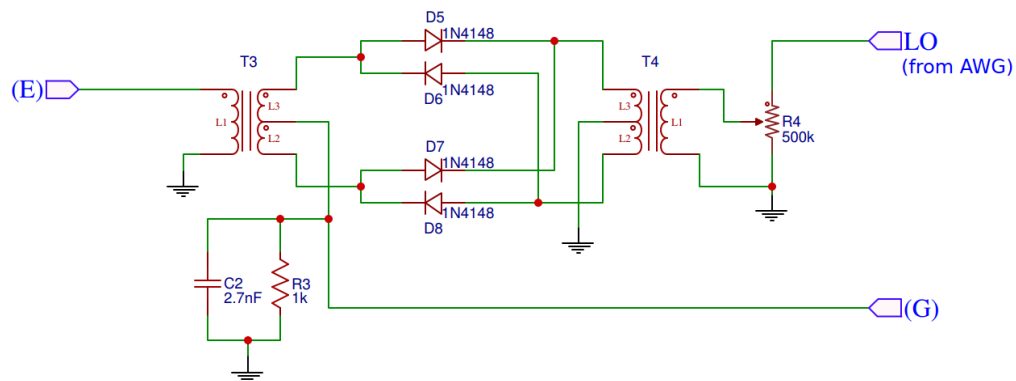


Figure 3.11: Circuit diagram of designed mixer. Label E represents one of the outputs from the receiver amplifier and G represents the mixer output. The Parallel attached R3 and C2 perform noise and high frequency filtering.

3.3.3 Audio Amplification

The low frequency output of the mixer is then amplified using an audio amplifier. This amplifier is designed using 741 integrated operational amplifier in feedback loop, generating a gain of ≈ 27 . Figure 3.12 is the circuit diagram of designed audio amplifier module running on 12 V and also fixed with high frequency filter in the input line. The amplified output is directly fed to the PC based oscilloscope for subsequent analysis. The two output channels from the pair of mixers are designated separate audio amplifier.

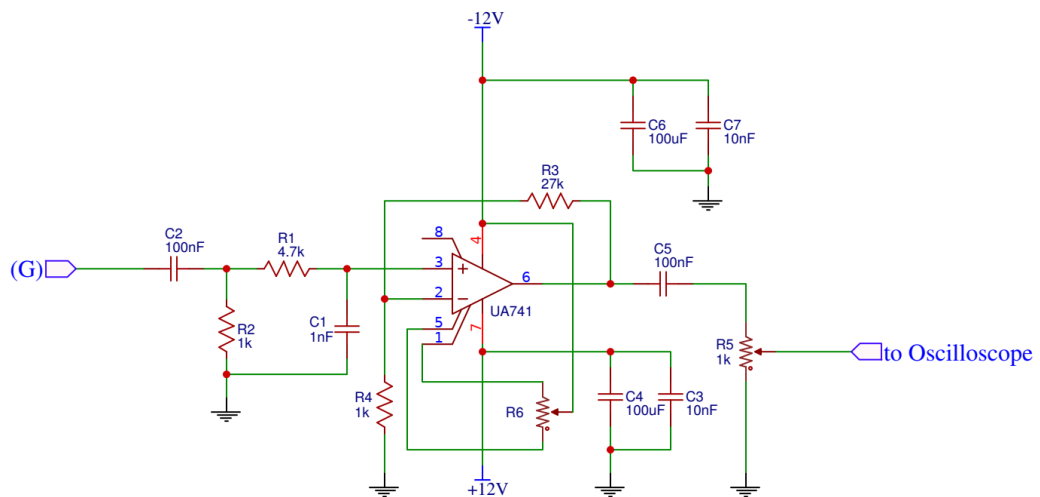


Figure 3.12: Circuit diagram of designed audio amplifier using 741 integrated operational amplifier. The gain adjusted to ≈ 27 and design allows for filtration of noise and higher frequencies.

Chapter 4

Results

In this chapter we present various test results from our devices and the final results taking from the samples. The results are captured on ZScope (ZT4611), with sampling frequency 4 GS/s max. and a 1000 points display window. For the experimental implementations we have tagged the circuit diagrams outputs and input channels, these connections are given in table *B.0.2* in appendix. PCB design for the designed circuit and complementary information of the probe and components can be found in appendix B. A conceptual diagram of the process of NMR is illustrated in figure 4.1, showing how the pulse is generated by overlapping gating pattern on the carrier pulse. The subsequent delay is provided before the acquisition of decaying signal.

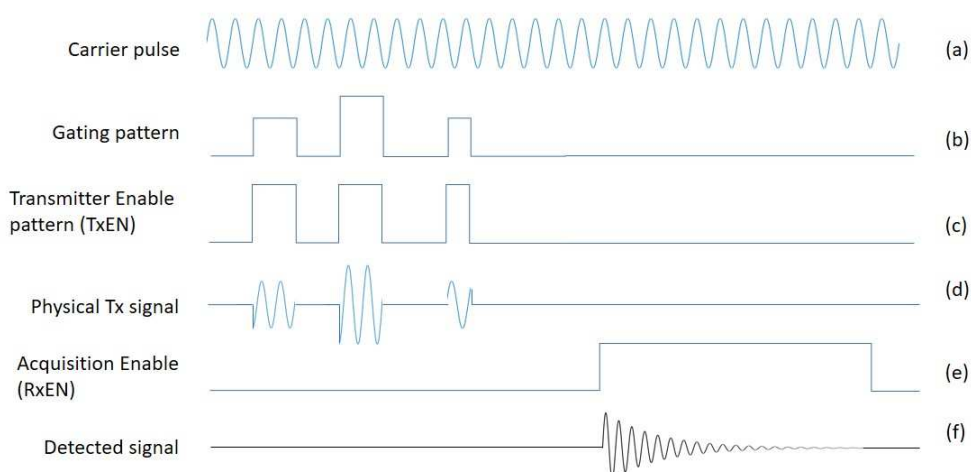


Figure 4.1: A conceptual illustration of the NMR process.

Fig 4.2 shows complete NMR setup used with Maran magnetic setup. This chapter includes the results in two categories, first section will show the timing and ampli-

fier component results and the second section includes all the components used in receiving, mixing and amplifying the signal.



Figure 4.2: Complete NMR system with Maran setup. Controlled distribution of power through power supply runs the amplifier circuits.

4.1 Transmit chain

4.1.1 Timing circuit

The timing circuit is operated with the trigger (Tr) from the computer interfaced AWG setup. The output ports A and B (in figure 3.2) provide receiver and transmitter enable pulses, respectively. The resulting pulse are captured on ZScope and the saved data is plotted in Matlab.

4.1.2 Transmitter amplifier

The designed transmitter amplifier works in pulsed mode with high frequency input and provides high power output for small time. The results of this amplifier, from C, is shown in fig 4.5

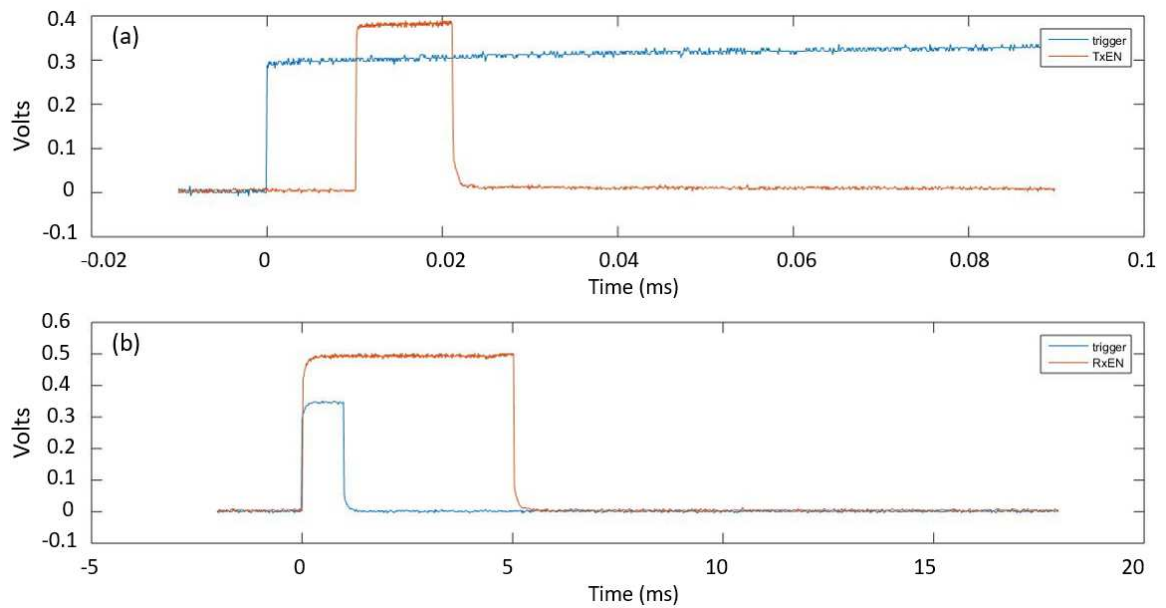


Figure 4.3: Plotted data of transmitter enable and receiver enable pulses. (a) show the transmission enable (TxEN) pulse along with rising edge of Trigger pulse. The delay between the two edges is $10\mu\text{s}$. (b) shows the receiver enabling pulse (RxEn, 5 ms) along with Trigger pulse.

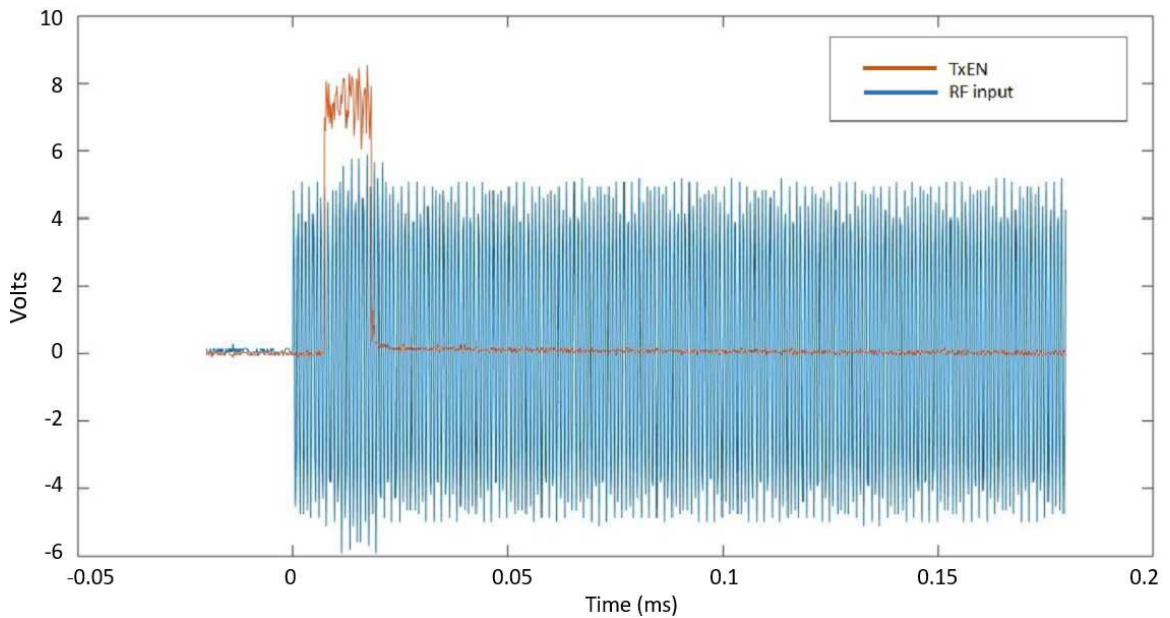


Figure 4.4: Transmitter test input, 5 V. The input frequency is 23.88 MHz. The amplification only takes place with in the enabling pulse, i.e., $10\mu\text{s}$

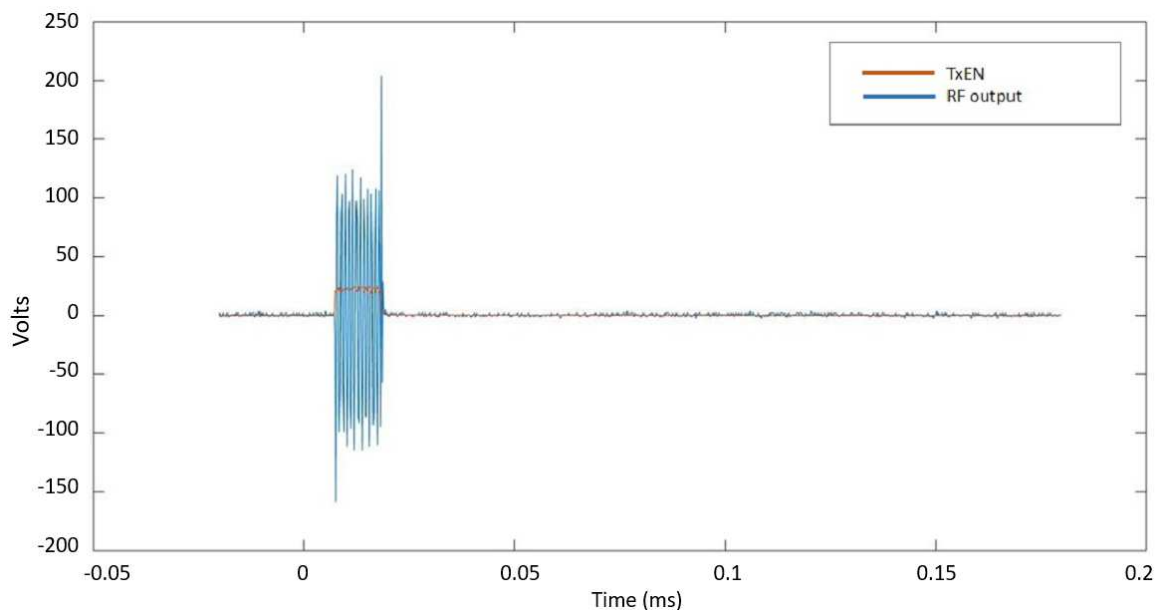


Figure 4.5: Resulting amplified output of the transmitter, from point C in the circuit diagram 3.3. The amplified output is 100 V. Note that the amplification and gating of the signal are simultaneous process.

4.2 Receive chain

4.2.1 Probe

The probe design information is mentioned in chapter 3. Probe tuning is the most important part of the entire NMR setup, which is also discussed in chapter 3. At a first glance it seems there is no output from the sample but, in fact, there is and this is precisely why we need amplification of the received signal. The results from the amplification of the test signal from Maran (23 MHz) magnetic setup are shown in Figure 4.6. The image show high amplitude pulse still existing at transmitter gate timing, it is the remaining excitation RF pulse crossing to the receive chain.

4.2.2 Pre-amplifier

The receiver amplifier is a dual stage amplifier as explained in chapter 3. The results achieved from the two stages are shown in Figure 4.7 and 4.8, respectively. The noise and high frequency filters in the amplifier circuit reduce the amplitude of RF signal with simultaneous increase in low frequency signal. The acquisition window for the receiver is 5 ms, subsequent to added time delay of $10\mu\text{s}$ from the falling edge of the transmit pulse.

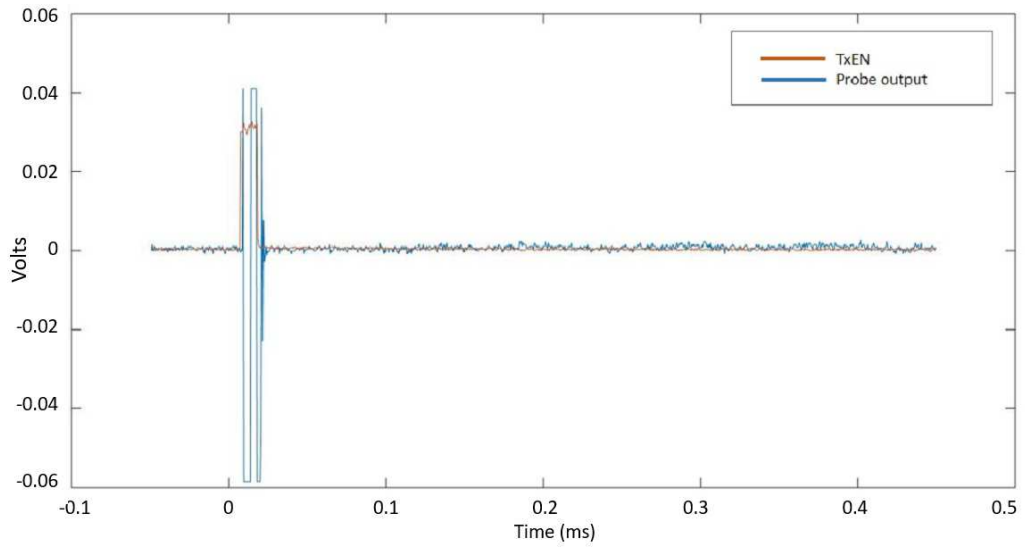


Figure 4.6: Probe output, point D, as taken from the Maran (23MHz) magnetic setup.

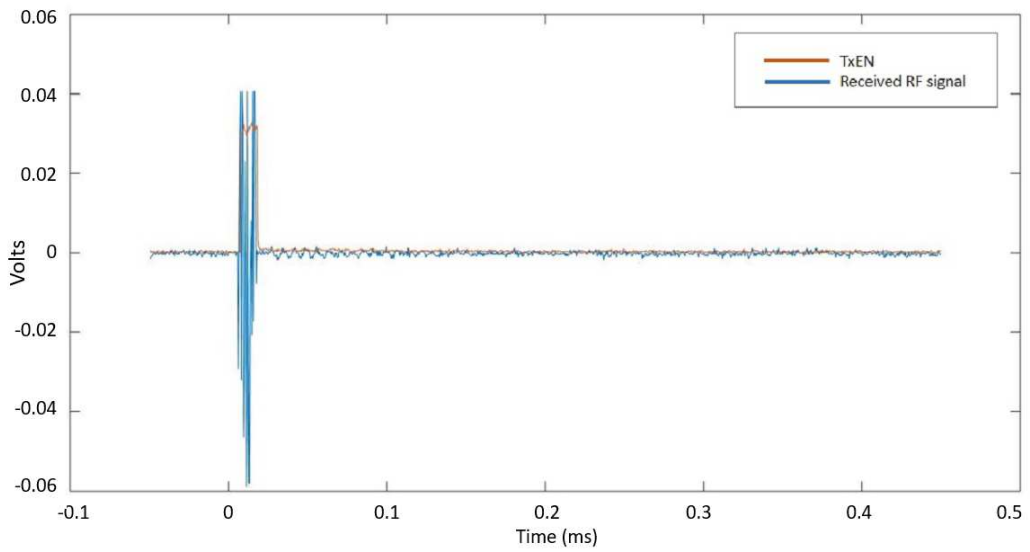


Figure 4.7: Amplified output from stage 1, which is point (i) in figure 3.9.

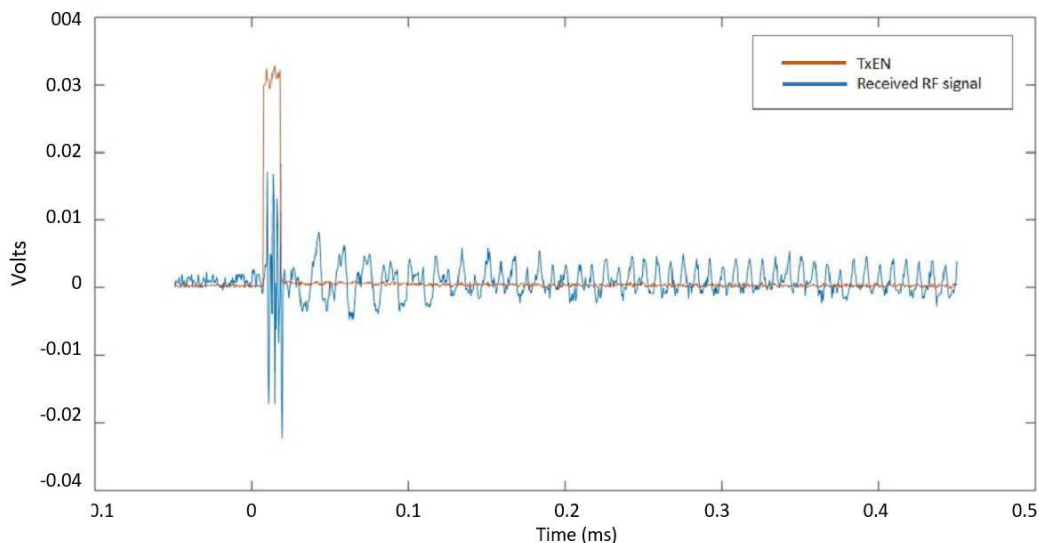


Figure 4.8: Amplified output from stage 2, which is point (ii) in figure 3.9.

4.2.3 Mixer

The mixer was employed to extract an audio signal from the received RF signal. The extraction is performed by recovering the difference signal of the mixer output while grounding the summed part. The result of our mixer, extracted from point G is shown in figure 4.9. When the whole assembly is connected in line we use two individual mixer circuits, both receiving 90° phase shifted f_o on LO port. In this scheme, E, from receiver amplifier is fed to mixer1 to produce resulting audio signal at port G while the signal on F is fed to mixer2 to produce resulting audio signal at port H. As described earlier, one of the output is called “real” and other “imaginary” both corresponds to channel- I and channel- Q , respectively.

4.2.4 Audio amplifier

Our final step in observing an FID is audio amplifier. The signal from the mixer output is fed to the audio amplifier, this signal is in KHz and exponentially decaying in nature. The channels I and Q are fed to two individual audio amplifier circuits. Figure 4.10 shows the output of I -channel audio amplifier from the final variable resistor.

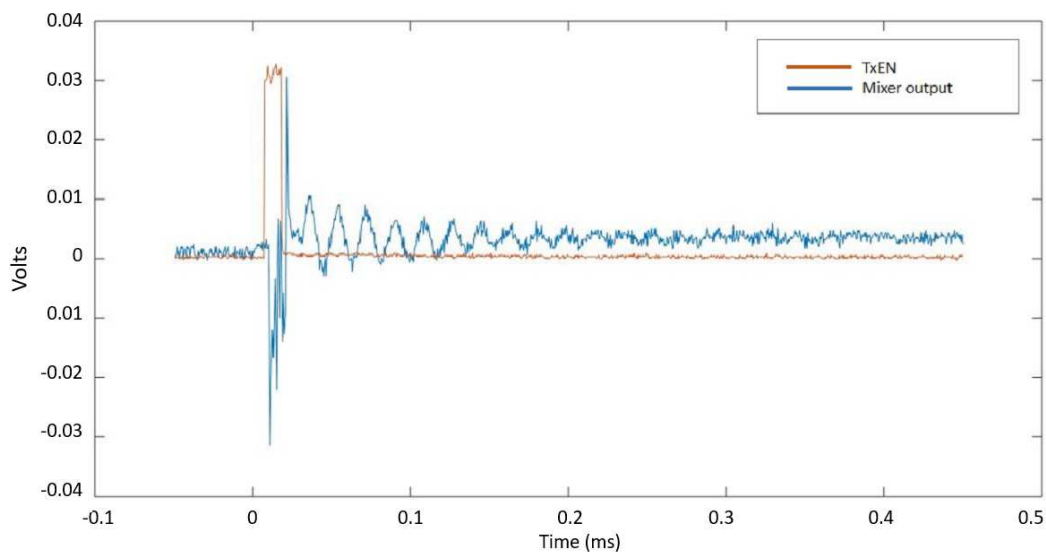


Figure 4.9: Mixer output in test pulse. The signal is filtered to output only the low frequency signal.

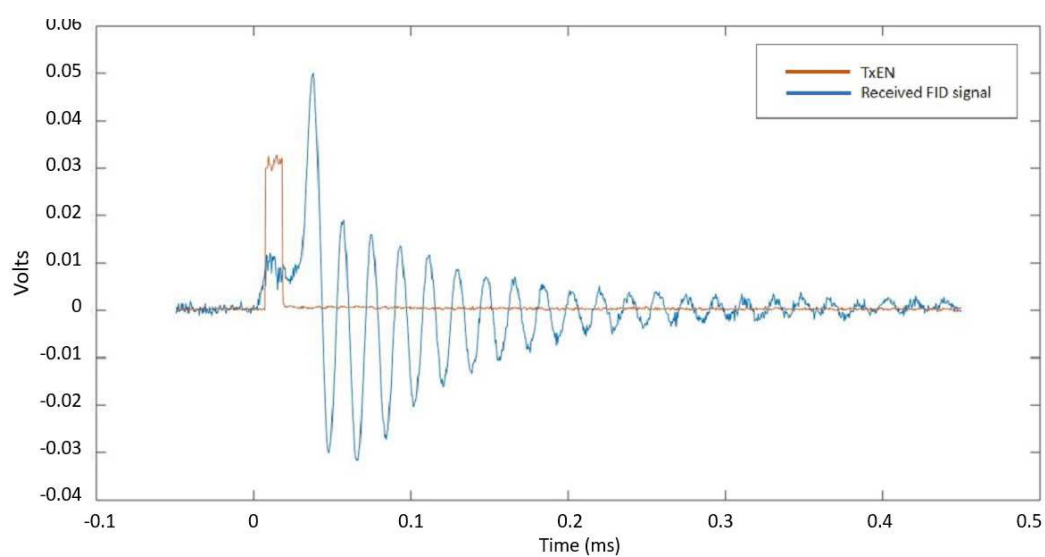


Figure 4.10: Amplified audio signal, this constitutes the final result as FID from the sample.

4.3 Sample results

So far we have shown the results from our running NMR setup with results from various points. We were able to test a few samples with Maran magnetic setup integrated with our transmit and receive chain devices. The results are collected through ZScope and plotted in Matlab. Following are the plots for ethanol, water and toluene, there FID curves. We have used the positive offsets of 600, 700 and 800

KHz in our experiments.

4.3.1 Ethanol

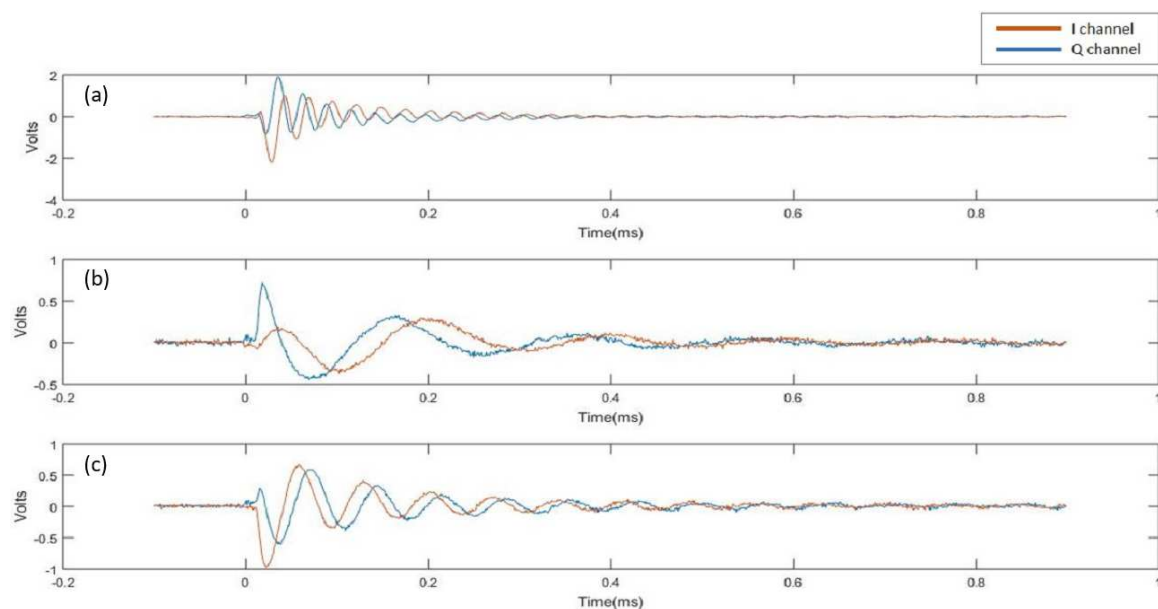


Figure 4.11: Free Induction Decay from ethanol sample. Plot (a) shows FID at offset 600KHz, plot (b) with offset 700KHz and plot (c) with offset 800KHz.

4.3.2 Water

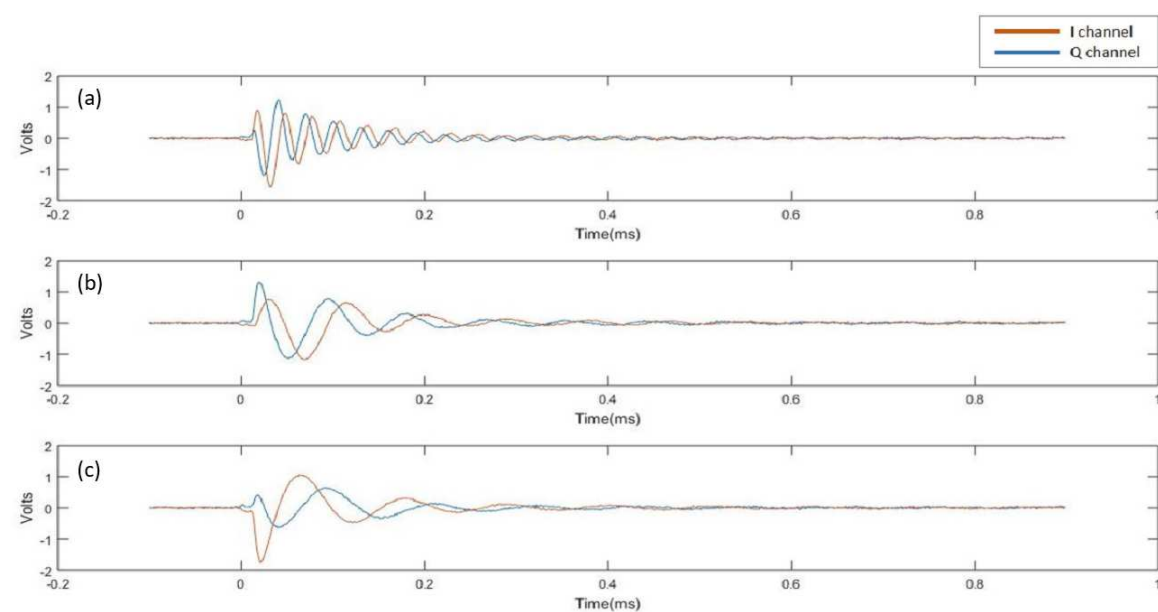


Figure 4.12: Free Induction Decay from water sample. Plot (a) shows FID at offset 600KHz, plot (b) with offset 700KHz and plot (c) with offset 800KHz.

4.3.3 Toluene

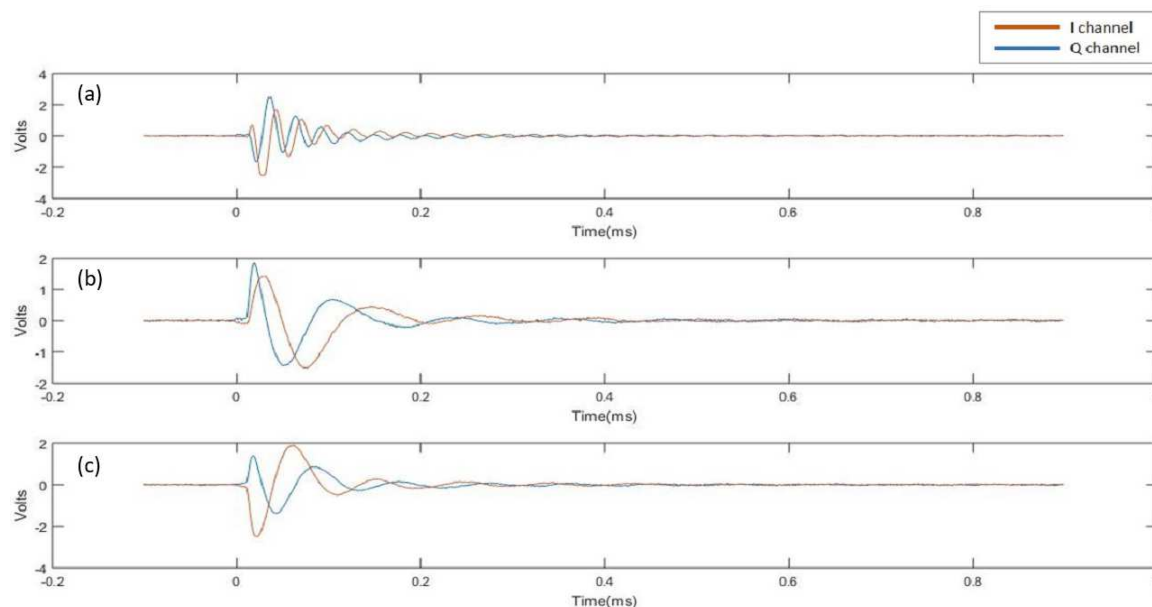


Figure 4.13: Free Induction Decay from toluene sample. Plot (a) shows FID at offset 600KHz, plot (b) with offset 700KHz and plot (c) with offset 800KHz.

4.4 Conclusion

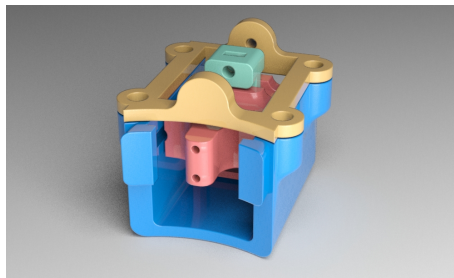
A low-field Nuclear Magnetic Resonance Spectrometer has been developed and demonstrated to receive Free Induction Decay from different samples. The developed system successfully demonstrate fundamental phenomenon at nuclear level. Current modular setup allowed working with two different magnetic setups. Hand made amplifiers and software package usage made the entire system cost effective. The transmission amplification was first made continuous then changed to triggered so a high powered pulse can be generated for small time consuming minimum power on average The use of pulse generators can be replaced by FPGA that can enhance the efficiency of the system to generate pulse sequence and process the NMR signal.

The resulting FID are fine quality and both channels are well distinguished in their phases. To this point, the inhomogeneity of the magnetic field restricts the resolving power of the spectrometer. The Fourier transforms of the results cannot resolve the peaks from ethanol and toluene samples. In future work, we see to design a homogeneous magnet to enable sufficient resolution NMR spectroscopy. we have also started to build an FPGA based solution for sample excitation and reception.

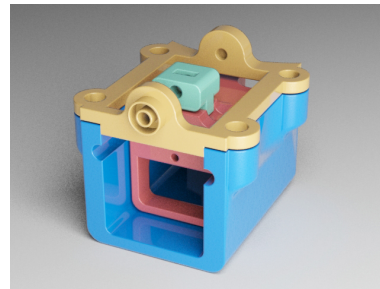
Appendix A

Design and PCBs

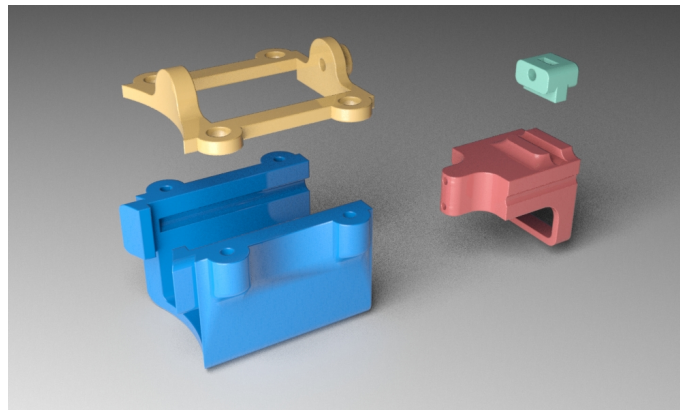
A.0.1 Probe



(a) Probe holder front view



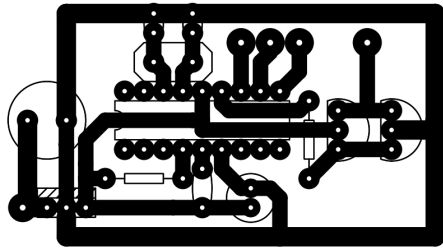
(b) Probe holder rear view



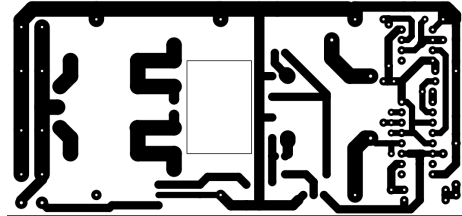
(c) Probe holder exploded view

Figure A.1: 3D printed probe holder used in with PM-1055 magnet.

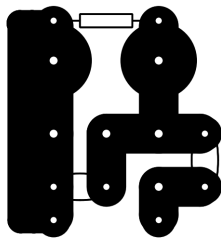
A.0.2 PCB design



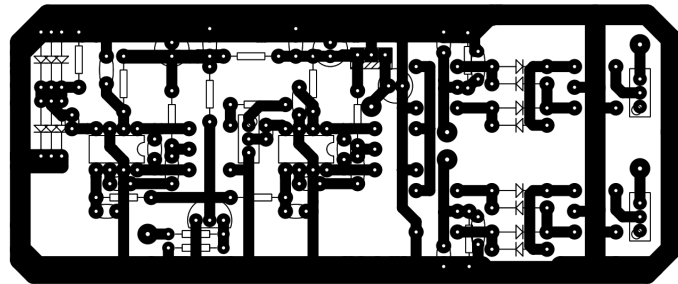
(a) Timing circuit



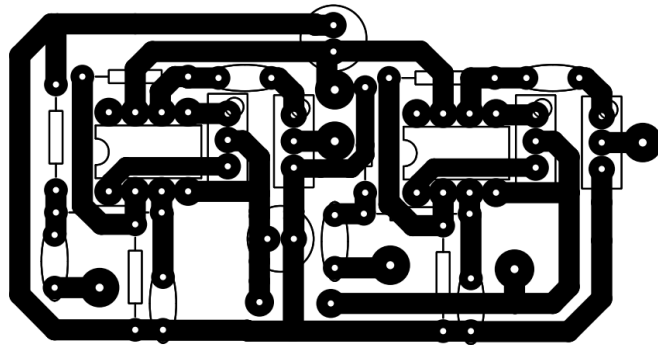
(b) Transmitter amplifier circuit



(c) Probe



(d) Receiver amplifier circuit & mixer



(e) Audio amplifier

Figure A.2: PCB design for all the components.

Appendix B

Components

B.0.1 List of abbreviations

Tag	Description
TrgIN	Trigger input
Tx	Transmitter
Rx	Receiver
RxEN	Receiver Enable (pulse)
TxEN	Transmitter enable (pulse)
TxAmp	Transmitter amplifier
RxAmp	Receiver amplifier
AWG	Arbitrary waveform generator
AGC	Automatic gain control

B.0.2 List of tags

Abbreviation	Full form	Figure reference
A	Receiver enable port	Fig 3.2
B	Transmitter enable port	Fig 3.2, 3.3
C	Amplified transmitter output port	Fig 3.2, 3.5
D	Probe (sample) output port	Fig 3.5, 3.9
E	Amplified received signal port (for I)	Fig 3.9, 3.12
F	Amplified received signal port (for Q)	Fig 3.9
G	Audio amplifier output port	Fig 3.2, 3.12, 3.13
I	Channel allocated for real part in FFT	
Q	90° degree phase shifted channel allocated for imaginary part of FFT	
i	First stage test point in receiver amplifier	Fig 3.9
ii	Second stage test point in receiver amplifier	Fig 3.9
Trg	Initiation Trigger pulse (from AWG)	

B.0.3 LabView probe tuning program

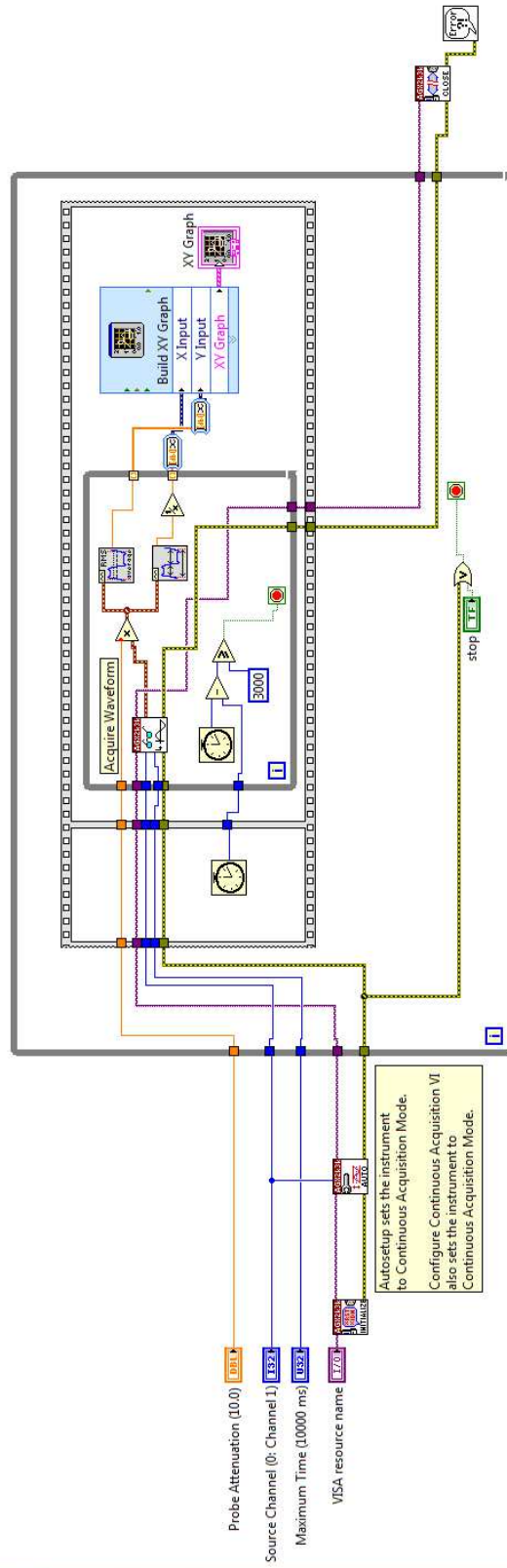


Figure B.1: Block diagram of probe tuning LabView program.

B.0.4 ICs



MOTOROLA

MC1350

Monolithic IF Amplifier

The MC1350 is an integrated circuit featuring wide range AGC for use as an IF amplifier in radio and TV over an operating temperature range of 0° to +75°C.

- Power Gain: 50 dB Typ at 45 MHz
50 dB Typ at 58 MHz
- AGC Range: 60 dB Min, DC to 45 MHz
- Nearly Constant Input & Output Admittance over the Entire AGC Range
- Y₂₁ Constant (-3.0 dB) to 90 MHz
- Low Reverse Transfer Admittance: << 1.0 μmho Typ
- 12 V Operation, Single-Polarity Power Supply

IF AMPLIFIER

SEMICONDUCTOR TECHNICAL DATA



P SUFFIX
PLASTIC PACKAGE
CASE 626

D SUFFIX
PLASTIC PACKAGE
CASE 751
(SO-8)



MAXIMUM RATINGS (T_A = +25°C, unless otherwise noted.)

Rating	Symbol	Value	Unit
Power Supply Voltage	V ⁺	+18	Vdc
Output Supply Voltage	V ₁ , V ₈	+18	Vdc
AGC Supply Voltage	V _{AGC}	V ⁺	Vdc
Differential Input Voltage	V _{in}	5.0	Vdc
Power Dissipation (Package Limitation)	P _D	625	mW
Plastic Package Derate above 25°C		5.0	mW/°C
Operating Temperature Range	T _A	0 to +75	°C

ORDERING INFORMATION

Device	Operating Temperature Range	Package
MC1350P	T _A = 0° to +75°C	Plastic DIP
MC1350D		SO-8

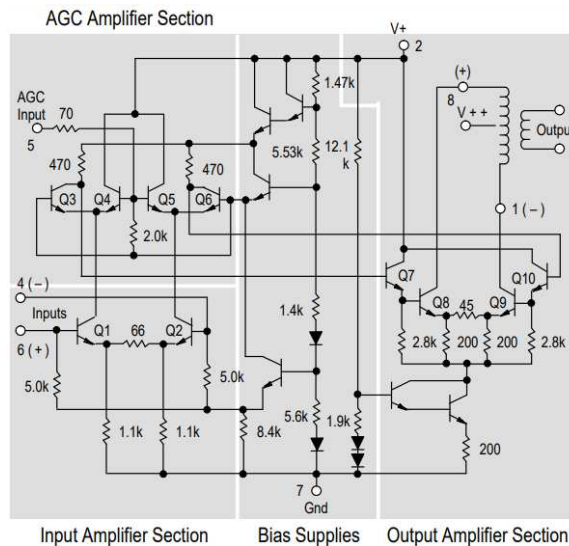


Figure B.2: MC1350 integrated circuit diagram revealing internal structure of the IC.

MC1350



PIC16F84A

18-pin Enhanced FLASH/EEPROM 8-Bit Microcontroller

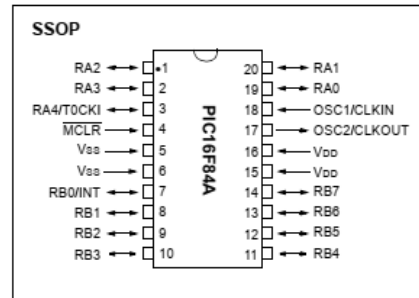
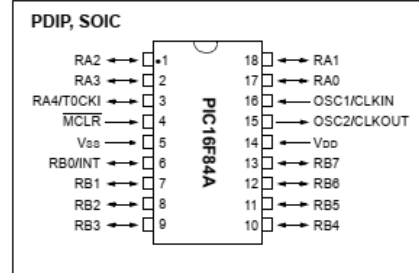
High Performance RISC CPU Features:

- Only 35 single word instructions to learn
- All instructions single-cycle except for program branches which are two-cycle
- Operating speed: DC - 20 MHz clock input
DC - 200 ns instruction cycle
- 1024 words of program memory
- 68 bytes of Data RAM
- 64 bytes of Data EEPROM
- 14-bit wide instruction words
- 8-bit wide data bytes
- 15 Special Function Hardware registers
- Eight-level deep hardware stack
- Direct, indirect and relative addressing modes
- Four interrupt sources:
 - External RB0/INT pin
 - TMR0 timer overflow
 - PORTB<7:4> interrupt-on-change
 - Data EEPROM write complete

Peripheral Features:

- 13 I/O pins with individual direction control
- High current sink/source for direct LED drive
 - 25 mA sink max. per pin
 - 25 mA source max. per pin
- TMR0: 8-bit timer/counter with 8-bit programmable prescaler

Pin Diagrams



PIC16F84 Device 16F84A

XTAL 4

Output PORTB

Input PORTA

High PORTB

LOOP:

Low PORTB.1

Low PORTB.0

DelayUS 7

High PORTB.0

DelayUS 5

High PORTB.1

DelayMS 5

Low PORTB.1

DelayMS 4000

BLF184XR; BLF184XRS

Power LDMOS transistor
Rev. 4 — 1 September 2015

AMPLEON
Product data sheet

1. Product profile

1.1 General description

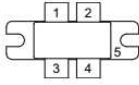
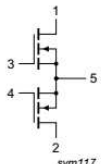
A 700 W extremely rugged LDMOS power transistor for broadcast and industrial applications in the HF to 600 MHz band.

Table 1. Application information

Test signal	f (MHz)	V _{DS} (V)	P _L (W)	G _p (dB)	η _D (%)
pulsed RF	108	50	700	23.9	73.5
CW	108	50	750	23.5	81.9

2. Pinning information

Table 2. Pinning

Pin	Description	Simplified outline	Graphic symbol
BLF184XR (SOT1214A)			
1	drain1		 sym117
2	drain2		
3	gate1		
4	gate2		
5	source ^[1]		

BLF184

Bibliography

- [1] P. J. Hore. “*Nuclear Magnetic Resonance*”, Oxford University Press, 2006.
- [2] S. Braun, H.-O. Kalinowski and S. Berger, “*150 and more Basic NMR Experiments*”, Wiley-Vich, 1998.
- [3] S.Appelt *et al.*, Phys. Rev. A **81**, 023420(2010).
- [4] Malcol H. Levitt, “*Spin dynamics: basics of nuclear magnetic resonance*”, John Wiley & sons, 2006.
- [5] E. Fukushima and Stephen B. W. Roeder, ”*Experimental pulse NMR: a nuts and bolts approach*’, Westview Press, 1981.
- [6] James Keeler, “*Understanding NMR Spectroscopy*”, John Wiley & sons, 2006.
- [7] M. P. Ledbetter *et al.*, arXiv: 1107.1706v1, 8 Jul 2011.
- [8] M. Carravetta, M.H. Levitt, J. Chem. Phys. 122, 214505 (2005).
- [9] M. Carevatta, O.G. Johannesen, M.H. Levitt, Phys. Rev. Lett. 92, 152003 (2004).
- [10] T. Jonischkeit, U. Bommerich, J. Stadler *et al*, Jour. Chem. Phys. 124, 201109 (2006).
- [11] P. Volegov, M. Flynn, R. Kraus *et al.*, IFMBE Proc. 28, 82-87 (2010).
- [12] M. Epsy, S. Baguisa, D. Dunkerley *et al.*, IEEE Trans. Appl. Supercond. 21, 530-533 (2011).
- [13] J-P. Korb, New Jour. Phys. 13, 035016 (2011).
- [14] F.G. Lynn, Mitchell Jonathan, New Jour. Phys. 13, 035001 (2011).
- [15] J. Hatta, M. Miyamoto and Y. Adachi, IEEE Trans. Appl. Supercond. 21, 526 (2010).

- [16] Liao Shu-Hsien; Chen Ming-Jye; Yang Hong-Chang; *et al.*, Rev. Sci. Instr. 81, 104104 (2010).
- [17] H. Dong, Y. Yang, S. Zhang, X. Xie, Supercond. Sci. Technol. 21, 115009 (2008).
- [18] J.N. Robinson, A. Coy, R. Dijkstra, C.D. Eccles, M.W. Hunter, P.T. Callaghan, Jour. Magn. Reson. 182, 343-347 (2006).
- [19] Callaghan P.T.; Halse M.E.; Coy A. et al., Jour. Magn. Reson.182, 75-83 (2006).
- [20] M. W. Hunter, R. Dykstra, M. H. Lim, T. G. Haskell and P. T. Callaghan, Appl. Magn. Reson. 36, 1-8 (2009).
- [21] Stephan Appelt, Holger Khn, F. Wolfgang Hsing and Bernhard Blmich, Nature Phys. 2, 105-109 (2006).
- [22] M. Hetrich, Progr. Nucl. Magn. Reson. Spectr. 53, 227-248 (2008).
- [23] F.R. Huson. "A desktop magnetic resonance imaging system. Magnetic Resonance Materials in Physics", Biology and Medicine, 13:177185, January 2002
- [24] D.M. Cole E. Esparza-Coss. "A low-cost mri permanent magnet prototype".
- [25] J. Kirsch and R. Newman. "A pulse nmr experiment for an undergraduate physics laboratory."
- [26] Zimmerman C.L., Boyden E.S., Wasserman S.C. (2010) "Classroom Nuclear Magnetic Resonance System". In: Herold K.E., Vossoughi J., Bentley W.E. (eds) 26th Southern Biomedical Engineering Conference SBEC 2010, April 30 - May 2, 2010, College Park, Maryland, USA. IFMBE Proceedings, vol 32. Springer, Berlin, Heidelberg
- [27] K. Rachineni, V. M. R. Kakita, Ramakrishna V. Hosur, RSC Adv., 2017, 7, 49102
- [28] J. R. Porter D.C. Spence E. Esparza D.C. Cole S.M. Wright, D.G. Brown and